

Comparative study of geometric properties of unreinforced PLA and PLA-Graphene composite materials applied to additive manufacturing using FFF technology



E. García ^{a,*}, P.J. Núñez ^a, J.M. Chacón ^b, M.A. Caminero ^a, S. Kamarthi ^c

^a Higher Technical School of Industrial Engineering, Energy Research and Industrial Applications Institute (INED), Department of Applied Mechanics and Project Engineering, University of Castilla-La Mancha, Avda. Camilo José Cela, s/n, 13005, Ciudad Real, Spain

^b Higher Technical School of Industrial Engineering, Institute of Applied Mathematics in Science and Engineering (IMACI), Department of Applied Mechanics and Project Engineering, University of Castilla-La Mancha, Avda. Camilo José Cela, s/n, 13005, Ciudad Real, Spain

^c Department of Mechanical and Industrial Engineering, Northeastern University, 360 Huntington Avenue, Boston, MA, 02115, USA

ARTICLE INFO

Keywords:

Graphene nanoplatelet reinforcement
PLA-Based composites
Dimensional accuracy
Flatness error
Surface texture
Surface roughness
Fused filament fabrication

ABSTRACT

In recent years, significant advancements in Fused Filament Fabrication (FFF) have enabled this technology to become one of the most leading techniques of Additive Manufacturing (AM) for the production of functional products. The poor mechanical properties of manufactured parts have traditionally imposed considerable limitations on use of FFF processes. These shortcomings have been overcome using new advanced filaments with nanoparticle reinforced components, short-length and continuous fibres, and other composite material processing technologies. Polymers reinforced with graphene nanoplatelets (GNP) have been an effective solution for improving electrical, thermal, and mechanical properties. However, the geometric properties of functional products manufactured with GNP reinforced polymers have not been analysed in spite of being crucial for the manufacture, assembly, and service life of functional products. The aim of this study was to compare an improved PLA polymer (PLA-3D) with a GNP reinforced PLA composite (PLA-Graphene) by analysing the geometric properties of dimensional accuracy, flatness error, surface texture, and surface roughness. The effect of the 3D printing parameters – build orientation (*Bo*), layer thickness (*Lt*), and feed rate (*Fr*) – on the geometric properties of two PLA-based filaments were evaluated. The results showed dimensional accuracy was mainly affected by the build orientation, where an increase in the layer area on the X-Y plane showing the highest dimensional deviation owing to the longer displacements of the extruder accumulating positioning errors. The dimensional accuracy along the Z-axis was not affected by any of the printing parameters nor the accumulation of layers, with results close to nominal ones. The flatness error and surface roughness were strongly conditioned by building orientation, with the best results obtained in the flat orientation. Neither of the compared materials showed significant variations between them in geometric properties, with similar results in the tested printing conditions.

1. Introduction

Fused Filament Fabrication (FFF) is rapidly becoming one of most extensively used technologies of Additive Manufacturing (AM) due to its simplicity, and the ability to manufacture thermoplastic polymers parts of great geometric complexity and shapes with high versatility and flexibility, but low material waste. Traditionally, FFF has been employed to manufacture only conceptual prototypes due to limitations in both the manufacturing process and the low mechanical properties of the

thermoplastic materials. In recent years, however, this technology has evolved exponentially and new materials with better mechanical properties have been developed, enabling FFF to become a viable alternative for manufacturing end-use products [1,2].

In FFF processes, the parts are built through the deposition of an extruded thermoplastic filament in successive individual layers until the final 3D geometry is achieved. To optimize the efficacy of the manufacturing process, a broad range of parameters must be configured; these parameters include layer thickness, build speed, feed rate, build

* Corresponding author.

E-mail address: eustaquio.garcia@uclm.es (E. García).

orientation, raster pattern, raster angle, raster width, temperature, among others [3]. They directly influence both the mechanical properties and geometric quality of manufactured parts [4]. The material is also an important aspect in FFF processes. The broad range of commercial thermoplastics available for FFF processes include acrylonitrile butadiene styrene (ABS), polylactic acid (PLA), polypropylene (PP), polyethylene (PE), polyamide (PA), polycarbonate (PC), polyetheretherketone (PEEK), and polyethylene terephthalate (PET), among others. Of these materials, ABS has been the most widely used material in FFF processes due to its good mechanical properties, wear resistance, high glass transition temperature, and impact resistance [5]. However, in the current search for environmentally friendly materials, PLA polymers have become a real alternative to ABS, primarily since PLA is derived from biomass, natural and renewable raw materials, and is not based on fossil fuels such as other thermoplastic (ABS). Moreover, other aspects such as lower cost, good mechanical properties, and reusability have made this polymer an ideal material for food, biomedical, aerospace, automotive, textile, and package engineering applications [6–9].

In spite of the substantial advantages of FFF over traditional manufacturing process, FFF often exhibits significant quality shortcomings, producing elements with lower mechanical properties and lower geometric quality. These drawbacks impose enormous limitations on the use of FFF. Because of this reason, traditional manufacturing processes are often preferred over additive manufacturing to achieve final products when high quality specifications are required. To overcome these drawbacks, polymer matrix composites have been developed to provide filaments with enhanced mechanical properties. Particles, fibres, or nanomaterials have been added as reinforcement to a polymer matrix, providing high performance filaments that are designed to improve the mechanical behaviour of manufactured products. In the literature, only a few studies have determined the effects of carbon and glass fibre reinforcements on the mechanical properties of parts manufactured by FFF [10]. Short fibre filaments have been used in most cases due to their ability to be extruded using the same printing techniques as those used for unreinforced thermoplastics; however, the study results showed only a slight enhancement in the mechanical behaviour of the fabricated samples [11–13]. The printing of continuous fibres has significantly improved the mechanical properties of unreinforced polymers, and increased filament performance, but this method has been applied to a lesser extent as it requires the use of specific 3D printers and more complex material processing [10,14].

The search for conductive materials with good thermal properties for manufacturing electronic devices by FFF processes has led to the addition of nanoparticles such as silver [15], copper [16] or graphene [17] to thermoplastic filaments. For example, the excellent mechanical, thermal and electrical properties of graphene make it an ideal reinforcement material for developing new composites for FFF processes. Recent studies have found incorporating graphene nanoplatelets (GNP) to polymer filaments was a promising technique for developing components requiring electrical and thermal conductivity [18,19]. Moreover, as reported by Caminero et al. [17], the addition of these nanoparticles was found to have a moderate impact on mechanical properties, with GNP slightly improving filament performance in terms of flexural and tensile stress as compared to unreinforced thermoplastics.

The potential capabilities of this incipient manufacturing technology have led to a proliferation of studies in the literature evaluating mainly the mechanical properties of different materials under diverse printing conditions. However, other critical aspect such as geometric properties have scarcely been examined, and the geometrical quality obtained with FFF processes still lags far behind the quality afforded by other manufacturing processes such as injection moulding, machining, casting, and forming [7,20,21]. Printing conditions have a decisive impact on geometrical quality as they directly influence extruded filament deposition and the material solidification procedure [4]. The erroneous selection of 3D printing parameters may lead to negative effects such as shrinkage and warping [22]. Thus, recent research has focused on

geometric quality characterization by evaluating 3D printing parameters, dimensional accuracy being the most researched parameter. García et al. [4] analysed the effect of the process parameters: build orientation, layer thickness, feed rate, and the plate-extruder precision motion in the dimensional accuracy of PLA using a low cost printer. Kumar et al. [23] and Sahu et al. [24] characterized dimensional errors on ABS-P400 by evaluating the 3D printing parameters: layer thickness, raster width, raster angle, part orientation, and air gap. Chang et al. [25] analysed images of ABS material to determine profile errors through the evaluation of the contour width effect, raster part width, contour depth, and raster angle. Peng et al. [26] studied how the process parameters: extrusion velocity, line width compensation, layer thickness, and filling velocity affected dimensional quality in FFF process with ABS material. Ahmed et al. [27] proposed an I-optimality criterion for the dimensional accuracy optimization of FFF processes evaluating the 3D printing parameters: build orientation, layer thickness, raster angle, air gap, number of contours, and road width. Kaveh et al. [28] optimized the printing parameters of extruded temperature and raster width for precision accuracy improvement on HIPS material. Geng et al. [29] developed an algorithm control for the microstructural dimensions of an extruded PEEK filament based on the analysis of extrusion speed and printing speed. Noriega et al. [30] improved the dimensional accuracy between parallel faces of ABS material modifying the theoretical dimensions of CAD models by new optimized values. Other important process parameters such as cooling air velocity have also had a considerable impact on dimensional accuracy, where higher values of this parameter improved geometric accuracy, as reported by Lee and Liu [31], but mechanical properties may deteriorate. Currently, the market offers a broad range of FFF printers, from low cost machines built with low precision elements to industrial equipment with high precision components. Galantuchi et al. [32] compared an industrial versus a low cost machine, obtaining elements with deficient dimensional precision with the low cost machine due to severe shrinkage in the fabricated parts. As reported by Spoerl et al. [22] in an extensive review on improvements in the dimensional accuracy and warping in material extrusion-based additive manufacturing of polypropylene, not only do the 3D printing parameters affect the dimensional accuracy, but also other aspects such as the geometry and the composition of the polymer severely influence shrinkage and warpage of parts fabricated by FFF. In order to overcome this drawback, several authors have suggested the use of fibre-reinforced polymers. Due to their low shrinkage properties, fibres reduce dimensional deviations and warpage [22]. Likewise, Spoerl et al. [33] found PP reinforced with short carbon fibres considerably experienced lower warpage than pure PP, as the addition of oriented and highly-conductive carbon fibres increased the conductivity of the material, enabling it to cool down homogeneously. In a further study of Spoerl et al. [34] the 3D-printed PP parts reinforced with expanded perlite spheres exhibited significantly reduced shrinkage, particularly with smaller fillers, leading to better dimensional accuracy of printed parts. Most of these studies, have only focused on the addition of reinforcements to semi-crystalline and high-crystallization rate (CR) materials like PP [35], as they tend to shrink and warp severely. However, the effect of reinforcements on the dimensional behaviour of low CR materials such as PLA has received little attention in the literature.

A further critical aspect of quality control for functional parts is the evaluation of form errors [36]; however, few studies have addressed this key aspect in FFF processes. As reported by García et al. [4], form errors were affected by both process parameters, and by the plate-extruder precision motion of FFF 3D printers. Mahmood et al. [37] developed an optimized Taguchi based process to examine the relationship between process parameters and geometric characteristics, and found that deviations were greater for holes, than for bosses on the X-Y plane. Reyes-Rodriguez et al. [38] evaluated the influence of the process parameters layer height, support strategy, and build direction on the shape deviations and dimensional accuracy of polycarbonate (PC), where form errors and deviations were influenced basically by build orientation,

whereas accuracy on the X–Y plane depended mainly on nozzle diameter. Núñez et al. [39] evaluated the influence of the process parameters fill density and layer thickness on dimensional accuracy and the flatness error with ABS-plus; they determined that the best dimensional behaviour was achieved with solid density and maximum layer thickness, and the lowest flatness error was obtained with solid density and less layer thickness. Sajan et al. [40] found that bed temperature, nozzle temperature, number of loops, infill, layer thickness, and print speed had a significant impact on the roundness error with ABS.

Moreover, surface finish has received little attention in the literature in comparison to dimensional accuracy. Ahn et al. [41] proposed a theoretical model of surface finish prediction in FFF processes using the printing parameters: surface angle, cross-sectional shape of the filament, layer thickness, and overlap interval. Similarly, Boscheto et al. [42] developed a theoretical model of surface finish using the process parameters: layer thickness, stratification angle, model filling, tilting, and support typology with ABS material. In a further study, Boscheto et al. [43] presented an innovative surface finish predictive model based on neural networks to overcome certain limitations [42]. Furthermore, these authors completed their previous studies with the analysis of other materials such as ABS plus, Ultem 9085, and Polycarbonate [44], and developed new methodology for embedding surface finish predictive models in the CAD design process [45]. Jin et al. [46] developed a mathematical model of surface profile and using the model they showed that good top surface quality was obtained in relation to the molten paste flow rate and the nozzle feed rate, and surface finishes on the sides were mainly influenced by layer thickness and the stratification angle. Analysing surface roughness in FFF processes using ABS, Reddy et al. [47] found that roughness decreased with increased build inclination, and increased with layer thickness. Occasionally, to improve the surface roughness in FFF processes, chemical [48] and heat treatments have been applied [18].

As mentioned above, research on geometric properties in FFF additive manufacturing has mostly focused on evaluating unreinforced thermoplastics, but new filament composite materials have been analysed to a lesser extent [22]. As mentioned above, only a handful of studies on composite polymers have observed promising results in improving dimensional accuracy. Thus, further studies on composite materials are required to evaluate not only dimensional accuracy, but also other key aspects of quality control such as form errors and texture surface given that reinforcements can severely affect these aspects. GNP reinforced thermoplastics such as PLA-Graphene are rapidly becoming a promising technique for the manufacture of components requiring good electrical, thermal, and mechanical properties. According to PLA-Graphene manufacturers, this composite material is supposed to provide better surface quality and closer tolerances than unreinforced PLA's, but to the best of our knowledge, no studies have been published supporting these claims. Only a preliminary study has been published [17], in which the addition of graphene to PLA-based composites did not significantly affect dimensional accuracy, and slightly improved surface roughness under certain printing conditions. This underscores the need for characterizing the effect of graphene nanoplatelet reinforcement of PLA-based composites to enhance mechanical, thermal, electrical, and geometric properties. Thus, the aim of this study was to perform an in-depth comparison of an unreinforced PLA with a GNP reinforced PLA in terms of the geometric properties of dimensional accuracy, flatness error, surface texture, and roughness. For an adequate characterization, two PLA-based filaments were analysed: a conventional. The effect of the 3D printing parameters – build orientation (*Bo*), layer thickness (*Lt*), and feed rate (*Fr*) – on the geometric behaviour of both PLA-based filaments were evaluated. The experimental data were analysed using analysis of variance (ANOVA), regression techniques, artificial neuronal networks, and response surfaces. Finally, surface texture and roughness 3D topography images were analysed to corroborate and confirm the mathematical models and response surfaces.

2. Experimental procedure

Two different commercial PLA-based filaments were analysed: (1) a modified PLA polymer filament (PLA-3D), SMARFIELD® PLA 3D850 natural, manufactured by Smart Materials 3D (Jaén, Spain); (2) and a HDPlas® PLA Graphene Nanoplatelet filament (PLA-Graphene) developed by Haydale Ltd. (Carmarthenshire, UK). PLA-3D is a polylactic acid filament specially designed for additive manufacturing and 3D printing applications; this filament increases the rate of crystallization, thermal resistance, and printing quality. In addition, this material provides less thermal contraction, and better mechanical properties than conventional PLA. PLA-Graphene is a PLA-based polymer with added functionalized graphene nanoplatelets ranging in size from 0.3 to 0.5 µm with 2% GNP loading. This composite filament improves mechanical properties and increases thermal conductivity, making this material suitable for electronic devices and components requiring high mechanical properties. Table 1 shows the comparison of the mechanical properties provided by the manufacturers of the two PLA-based materials used in this study.

This study was developed using a low cost FFF 3D printer BQ Witbox (Spain) specifically designed for producing parts using of PLA-based materials. This 3D printer uses a control system compatible with any open source software. In this study, the software selected for controlling the process parameters and generating the G-code was Ultimaker Cura. As mentioned in the introductory section, three printing parameters – feed rate (*Fr*), layer thickness (*Lt*), and build orientation (*Bo*) – were varied while keeping other parameters constant to determine their influence on the geometric characteristics of the PLA-based materials under study. The PLA-based filament diameter was 1.75 mm with a 0.4 mm nozzle size. A 100% solid fill density was selected as it was the most desirable material density for functional components requiring optimal mechanical properties. A full factorial design with three factors at different levels was carried out for printing the samples: *Fr* at three levels (20, 50, and 80 mm/s); *Lt* was evaluated at four levels (0.06, 0.12, 0.18, and 0.24 mm); and *Bo* at three levels (flat, on-edge, and upright orientations).

The flat, on-edge, and upright build orientations (F, O, U) are shown in Fig. 1. These three orientations were designed to evaluate the effects of accumulated layers, the sample stability of different support areas, and the impact of the extrusion length (X–Y plane) on geometric properties. As shown in Fig. 1, the coordinate system was defined according to the direction of the extruder: X-axis and Y-axis for longitudinal and transversal movements on the plane of the build plate, respectively; and the Z-axis for vertical displacement perpendicular to the build plate.

A Coordinate Measuring Machine (CMM) Tesa Micro-Hite (Switzerland) provided with PC-DMIS software was used for the dimensional deviation measurements (Fig. 1). The CMM has a resolution of 0.001 mm, with a repeatability $R(x, y, z) = 0.004 + 0.005L/1000$, where *L* is the machine axis length (*X* = 457 mm, *Y* = 508 mm, *Z* = 406 mm). The dimensions of each sample were assessed on the three manufacturing axes (X, Y, and Z) as the distance between parallel planes. Each sample plane was measured using a 3D stylus Tesastar-i with a 2 mm diameter ball. Because the measurement planes vary in size, the sampling points were measured as follows: In orientation 1 and 2, which have bigger sampling areas, 10 points were taken; whereas in

Table 1
Mechanical properties of PLA-3D, and PLA-Graphene filaments.

Mechanical Properties	PLA-3D	PLA-Graphene
Tensile modulus (MPa)	3510	3752
Tensile strength (MPa)	53.4	66.8
Flexural Modulus (MPa)	2404	2450
Flexural strength (MPa)	98.4	98.5
Elongation at break (%)	4.4	2.6
Izod Impact strength (J/m)	34.6	40.4
Density (g/m ²)	1.24	1.11

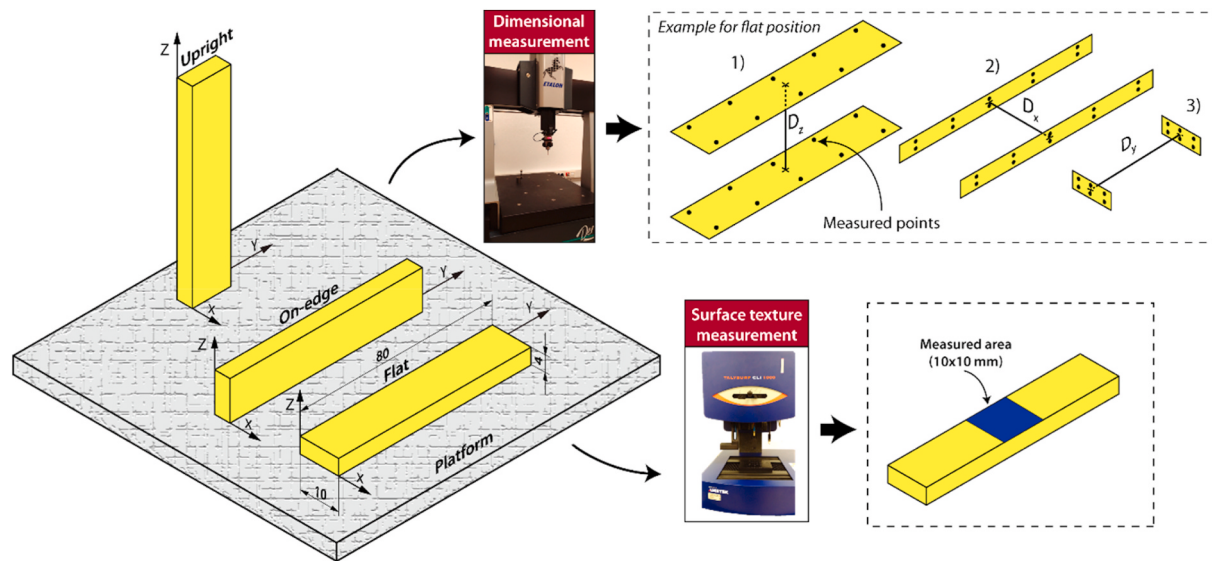


Fig. 1. Experimental procedure description for dimensional, form, and surface texture quality control.

orientation 3, which has a smaller sampling area, only 6 points were taken (Fig. 1). The dimensional deviations (ΔD_i) on the three manufacturing axes were defined as $\Delta D_i = L_n - L_e$, where L_n is the nominal length provided by Ultimaker Cura software, L_e is the measured length obtained with CMM, and i is the index of each respective measurement axes (X, Y, or Z).

Flatness, surface texture, and roughness were assessed with a 3D surface profilometer system (Talysurf CLI-1000) with a high-resolution (40 nm) contact inductive gauge (United Kingdom). An area of 10 × 10 mm², located in the middle of the face's largest surface of each sample was measured. Flatness was evaluated with the *root mean square flatness deviation* ($Fltq$) parameter [49]. Surface roughness was assessed with the *arithmetic mean height* Sa , and the *maximum height of peaks and valleys* Sz parameters by using a Gaussian low-pass filter at 0.8 mm cut-off (λ_c) [50].

The $Fltq$ parameter (eq. (1)) was defined as the square root of the sum of the squares of the local flatness deviations from the *Least Squares Reference Plane* [49],

$$Fltq = \sqrt{\frac{1}{A} \int_A LFD^2 dA}, \quad (1)$$

where LFD is the local flatness deviation, and A is the flatness area of the geometric element. The Sa parameter (eq. (2)) quantified the deviations in the height of the surface points in relation to the *Mean Reference Plane*

[50],

$$Sa = \frac{1}{A} \iint_A |z(x, y)| dx dy, \quad (2)$$

where A is the measurement area. The Sz parameter (eq. (3)) is defined as the sum of the largest peak height value and the largest pit depth value within the defined area [50],

$$Sz = \max(z(x, y)) + \min(z(x, y)). \quad (3)$$

3. Result and discussion

3.1. Dimensional characterization

Dimensional accuracy was assessed along the three orthogonal axes (X, Y, Z) which define the extruder movements. Table 2 shows for both the PLA-3D and PLA-Graphene filaments, the best regression models for dimensional accuracy (ΔD_x , ΔD_y , ΔD_z) as functions of the 3D printing parameters (Fr , and Lt) for each measured direction (X, Y, Z), and build orientation (F, O, U). The model goodness of fit was quantified by determination coefficient R_{adj}^2 , and the Pearson correlation coefficient (PCC). In several cases, the regression models obtained small R_{adj}^2 values, which revealed that dimensional behaviour was not adequately characterised by regression models. This poor model fit was mainly due to

Table 2

Adjusted coefficient of determination (R_{adj}^2), and Pearson's correlation coefficient (PCC) for dimensional deviations.

Material	Axis	Parameters	Build Orientation					
			Flat		On-edge		Upright	
			$R_{adj}^2(\%)$	PCC	$R_{adj}^2(\%)$	PCC	$R_{adj}^2(\%)$	PCC
PLA-3D	X	Fr	47.8	-0.798	25.9	-0.379	48.3	0.146
		Lt		0.084		0.636		0.761
	Y	Fr	57.4	-0.794	97.8	0.400	51.1	0.123
		Lt		-0.091		0.851		-0.372
PLA-Graphene	Z	Fr	21.6	0.504	35.9	-0.711	1.4	0.170
		Lt		0.485		-0.049		-0.157
	X	Fr	97.6	-0.082	64.0	-0.464	91.8	0.060
		Lt		0.978		0.610		0.940
	Y	Fr	85.9	0.001	96.5	0.479	81.9	-0.436
		Lt		0.957		0.843		-0.700
	Z	Fr	10.0	-0.200	84.6	-0.041	63.1	-0.153
		Lt		-0.227		-0.839		-0.811

the smaller PCC values, ranging ± 0.5 in many cases, which indicated lack of linear relationship between dimensional accuracy (ΔD_x , ΔD_y , ΔD_z) and the 3D printing parameters (Fr , and Lt). The poor results indicated the regression models are inadequate for characterizing dimensional accuracy.

Thus, artificial neural networks (ANN), which are known to capture non-linear relationships among inputs and outputs, were employed to model the behaviour of dimensional deviations with respect to process parameters. In order to show uniform results and establish an effective comparison, both the PLA-3D and the PLA-Graphene filaments were characterized by ANNs. The ANNs were trained using the feed-forward back-propagation algorithm, and the best network results were obtained with the Levenberg-Marquardt training function, the hyperbolic tangent transference function, and a 2-8-4-1 network structure. The two inputs to the ANN were Fr and Lt and the output is ΔD_x , ΔD_y , or ΔD_z . Once the ANN parameters (weights and biases) were obtained, surface responses (Fig. 2) were represented individually for each measurement direction (X, Y, Z) and build orientation (F, O, U), and the corresponding change in dimensional deviations (ΔD_x , ΔD_y , ΔD_z), and their tolerances to the processing parameters, Fr and Lt , were evaluated. Dimensional deviations are denoted as $\overline{\Delta D}_i(SD)$, where $\overline{\Delta D}_i$ is the mean dimensional deviation on each axis ($i = X, Y$, or Z), and (SD) is the standard deviation of experimental value samples. The tolerances (Tol) represent the difference between the maximum and the minimum values obtained for each axis and orientation.

Fig. 2 shows the surface responses obtained for dimensional deviation on the X-axis (ΔD_x) for both the PLA-3D and the PLA-Graphene filaments, with the upright and on-edge orientations showing the best behaviour with the smallest deviations. In the upright orientation, both materials obtained a similar quasi-plane response surface, with no significant influence of feed rate, and a small increase in dimensional error with increasing layer thickness. The dimensional deviation tolerances were very similar for both cases, 189.5 μm for PLA-3D (Fig. 2c), and 206.5 μm for PLA-Graphene (Fig. 2f), with the mean dimensional deviations of 53.9(62.2) μm , and 68.1(73.3) μm , respectively. These results showed the lowest deviations of the three building orientations. Both

materials obtained optimum results, with dimensional error values close to nominal ones in the smallest layer thickness, except for PLA-3D at an intermediate feed rate, where a slight increase in dimensional error was detected.

For the on-edge orientation, the results were very similar to those of the upright orientation. The PLA-Graphene (Fig. 2e) obtained a quasi-plane response surface, with a dimensional deviation tolerance ΔD_x of 210.5 μm , and a mean dimensional deviation of 73.9(64.3) μm . Once again, the best results reached dimensional deviation values close to nominal ones in the thinnest layer thickness with no influence of feed rate. The PLA-3D (Fig. 2b) also obtained a similar response surface with a dimensional deviation tolerance ΔD_x of 208.5 μm , but with higher dimensional error values than those for the PLA-Graphene, particularly in large layer thicknesses, reaching a mean dimensional deviation of 123.2(73.4) μm .

The flat orientation significantly increased the dimensional deviations of both materials. The PLA-3D (Fig. 2a) exhibited a non-uniform behaviour with ΔD_x values ranging from 163.6 μm to 488.3 μm (Tol = 324.7 μm), and a mean dimensional deviation of 326.9(110.9) μm . In this case, a clear pattern of the influence of 3D printing parameters could not be determined, the best results were obtained with the smallest layer thickness and highest feed rate. The PLA-Graphene (Fig. 2d) showed a different behaviour, with higher dimensional errors ranging from 301.3 μm to 790.6 μm (Tol = 489.3 μm), and a mean dimensional deviation of 540.6(166.1) μm . This material showed a clear tendency of increasing dimensional error with increasing layer thickness, and no influence of feed rate.

Thus, the results revealed that dimensional accuracy was mainly influenced by the length of the movement of the extruder. In the flat orientation, with longer X-axis displacement, the errors sharply increased with higher tolerances when compared to the on-edge and upright build orientations. In contrast, only the flat orientation showed differences in behaviour between the two materials analysed, particularly with large layer thicknesses where PLA-Graphene obtained very high tolerances due to deficient solidification of layers that produced irregular surfaces in all tested samples.

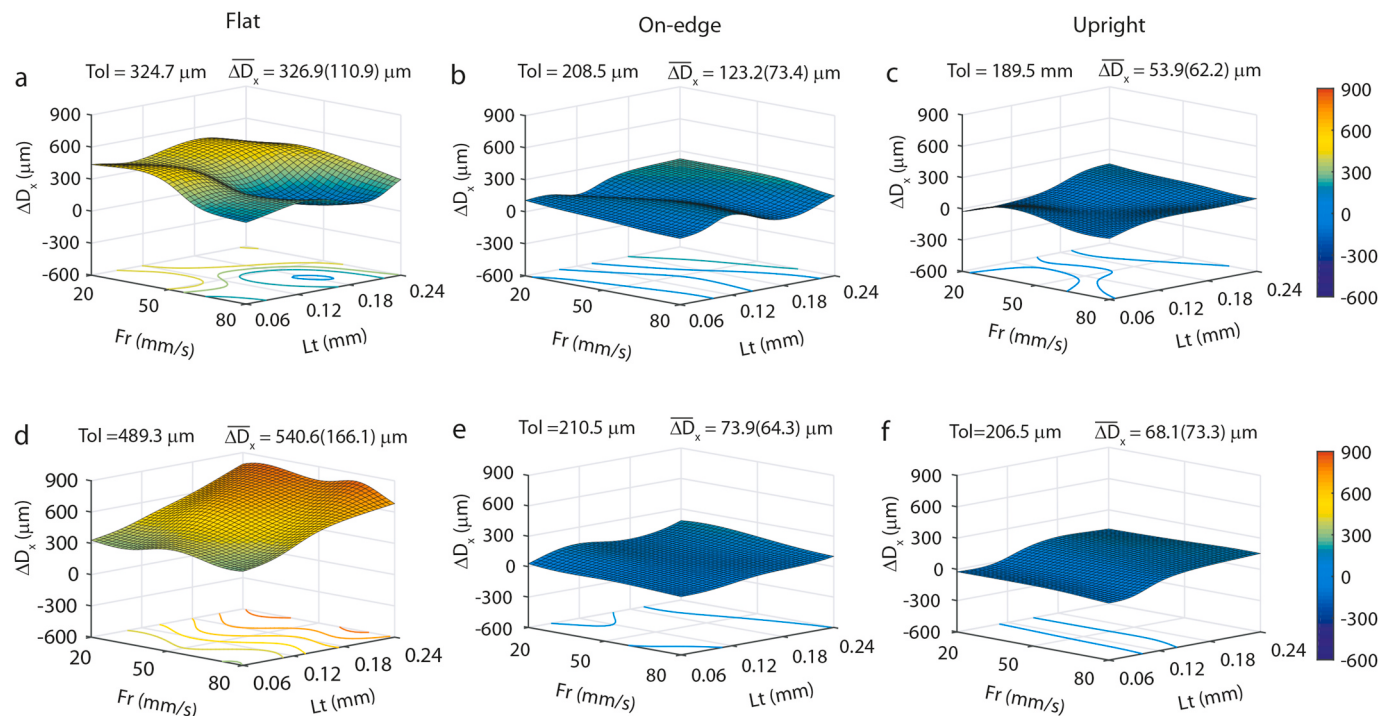


Fig. 2. Response surface obtained by ANN for X-axis dimensional deviation in the three building orientations. PLA-3D: flat (a), on-edge (b), and upright (c); and PLA-Graphene: flat (d), on-edge (e), and upright (f).

Fig. 3 shows the surface responses for the dimensional errors in the Y-direction (ΔD_y) for both the PLA-3D and PLA-Graphene filaments. The upright orientation once again obtained the best behaviour, particularly for the PLA-3D (**Fig. 3c**), where minimum dimensional deviations were very close to nominal ones. The maximum and minimum dimensional deviations were 92.6 μm and -76.6 μm respectively (Tol = 169.2 μm), with a mean dimensional deviation of -12.5(53.9) μm . The feed rate had no significant effect on dimensional errors, with only a slight increase in ΔD_y values for smallest layer thickness; the best results were obtained at the highest layer thickness. The PLA-Graphene in the upright orientation (**Fig. 3f**) performed similar to PLA-3D, but obtained higher ΔD_y values with smaller layer thicknesses, increasing dimensional tolerance to 257.3 μm , and the mean dimensional deviation to 54.3 (80.9) μm . For PLA-Graphene, the optimum dimensional deviation was observed at an intermediate layer thickness of 0.12 mm.

The on-edge orientation exhibited similar behaviour for both the PLA-3D (**Fig. 3b**) and PLA-Graphene (**Fig. 3e**) filaments, with negative dimensional error values in most cases. In this orientation, higher dimensional tolerances of 500.0 μm and 539.9 μm , and higher mean dimensional deviations of -261.2(157.7) μm and -140.3(174.3) μm , were found for PLA-3D and PLA-Graphene, respectively. In general terms, increased layer thickness positively affected and improved the dimensional accuracy of both materials, in particular with medium to high feed rates, reaching an optimum of -40 μm for PLA-3D, and -54 μm for PLA-Graphene at $Fr = 50 \text{ mm/s}$, and at $Lt = 0.24 \text{ mm}$ and $Lt = 0.18 \text{ mm}$, respectively.

The behaviour in the flat orientation was different for the two materials under study. The PLA-3D (**Fig. 3a**) obtained a moderate distribution in all of the process parameters under study, with a mean deviation of -68.7(125.1) μm , and ΔD_y values in the range of 108.6 μm to -280.3 μm (Tol = 388.9 μm). The optimum deviation ΔD_y of -25 μm was obtained with both the smallest layer thickness (0.06 mm) and medium feed rate (50 mm/s), and the slowest feed rate (20 mm/s) and largest layer thickness (0.24 mm). In contrast, the PLA-Graphene (**Fig. 3d**) depicted a completely different behaviour, with dimensional errors close to nominal ones for the small layer thicknesses (0.06 mm and 0.12 mm) in all evaluated feed rates. However, with medium and

large layer thicknesses a higher quasi-linear increase was obtained, increasing tolerance to 464.3 μm , with a mean dimensional deviation of 205.3(171.2) μm . Similar to the case of X-axis, the higher tolerances on the Y-axis were produced with the longer displacement of the extruder, i.e. flat and on-edge build orientations. In addition, the greatest differences between tested materials were obtained once again in the flat orientation.

As shown in **Fig. 4**, in general terms, the analysis of dimensional accuracy on the Z-axis of both the PLA-3D and PLA-Graphene filaments showed better behaviour than on the X-Y axis in all of the build orientations, except for the PLA-3D on-edge orientation with a moderate increase in tolerance. In the analysis of the flat orientation, the PLA-3D (**Fig. 4a**) showed better results than the PLA-Graphene, with lower dimensional errors ranging from 13.5 μm to -155 μm (Tol = 168.5 μm), and a mean dimensional deviation of -72.6(59.6) μm . An optimum dimensional deviation of 2 μm was found with $Fr = 50 \text{ mm/s}$ and $Lt = 0.18 \text{ mm}$. The PLA-Graphene (**Fig. 4d**) showed greater variability, with values below the nominal dimension in most of the 3D printing conditions under analysis. Tolerance increased to 264.0 μm , and the mean deviation value increased to -140.1(41.6) μm , achieving an optimum value of -31.3 μm with $Fr = 20 \text{ mm/s}$ and $Lt = 0.12 \text{ mm}$.

In contrast to the flat build orientation, in the on-edge orientation, the PLA-Graphene (**Fig. 4e**) was the material with the best behaviour, showing a quasi-plane distribution with no significant influence of the printing parameters. This filament material obtained a tolerance close to 141.0 μm , a mean dimensional deviation of -55.9(41.4) μm , and an optimum dimensional deviation of -8.6 μm at $Fr = 80 \text{ mm/s}$ and $Lt = 0.06 \text{ mm}$. Similar to the flat orientation, the dimensional values obtained were below nominal dimensions in most cases for PLA-Graphene, but to a lesser extent. PLA-3D (**Fig. 4b**) showed greater dimensional deviations, a higher tolerance of 476.6 μm , and a mean dimensional deviation of 22.6(129.5) μm . This material reached an optimum of -1.6 μm with $Fr = 16 \text{ mm/s}$ and $Lt = 0.18 \text{ mm}$.

The upright orientation showed good results for both filaments, with tolerances close to 193.2 μm and 197.9 μm , and a low mean dimensional deviation of -6.4(55.2) μm and 45.0(65.2) μm for PLA-3D (**Fig. 4c**) and PLA-Graphene (**Fig. 4f**), respectively. The best dimensional accuracy

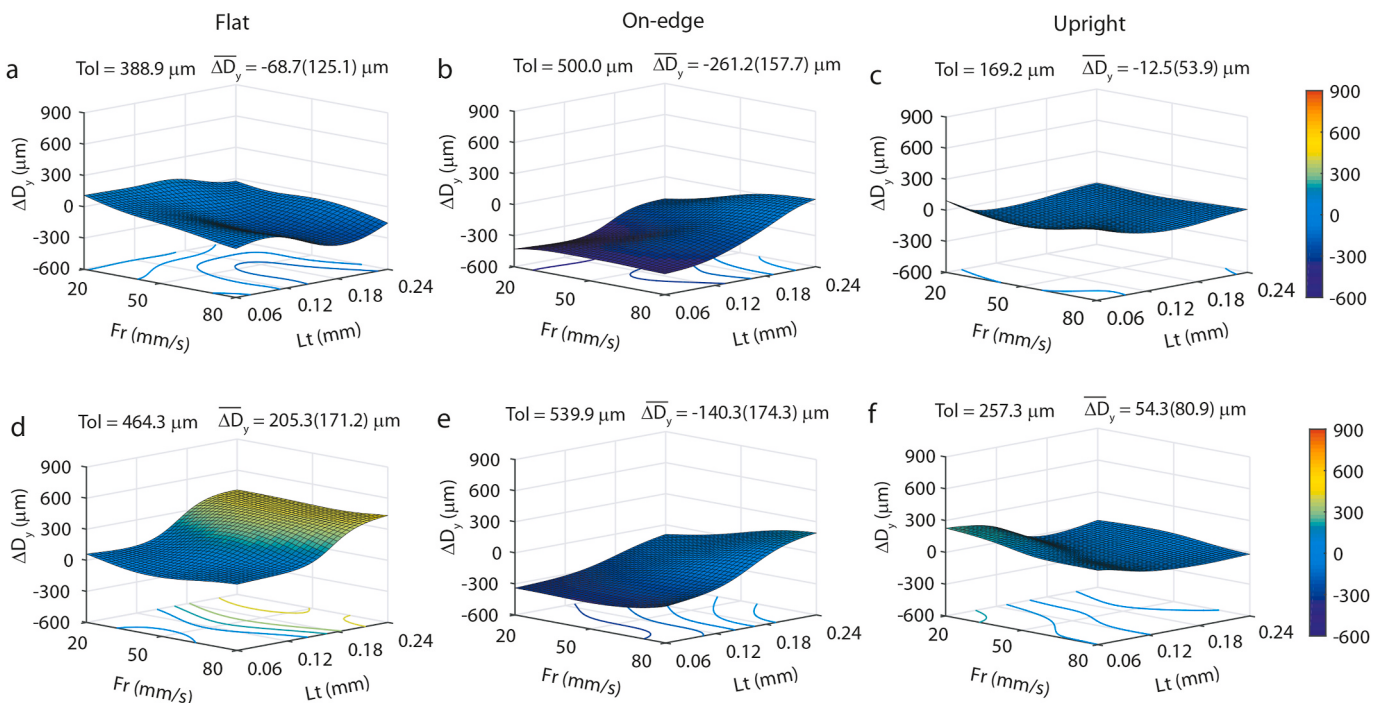


Fig. 3. Response surface obtained by ANN for Y-axis dimensional deviation in the three building orientations. PLA-3D: flat (a), on-edge (b), and upright (c); and PLA-Graphene: flat (d), on-edge (e), and upright (f).

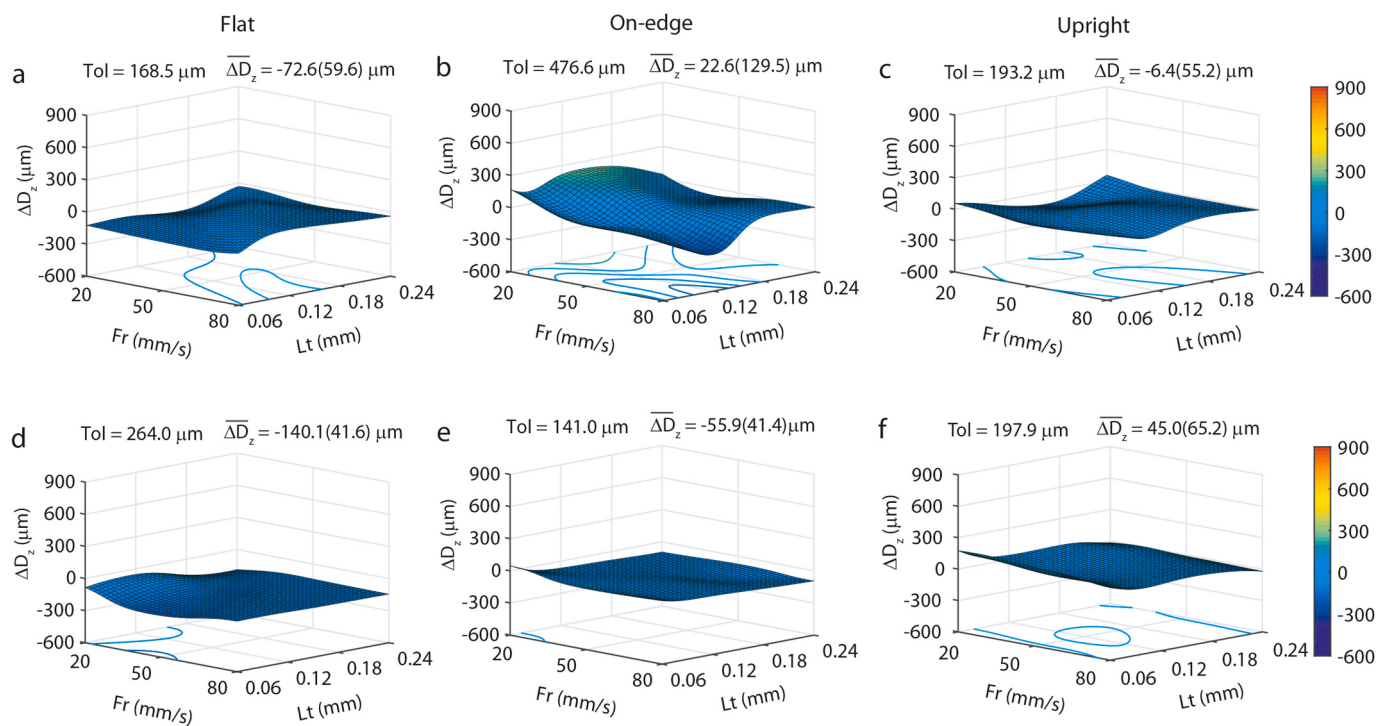


Fig. 4. Response surface obtained by ANN for Z-axis dimensional deviation in the three building orientations. PLA-3D: flat (a), on-edge (b), and upright (c); and PLA-Graphene: flat (d), on-edge (e), and upright (f).

was 2.6 μm with $Fr = 80 \text{ mm/s}$ and $Lt = 0.12 \text{ mm}$ for the PLA-3D filament, and 0 μm with $Fr = 50 \text{ mm/s}$ and $Lt = 0.18 \text{ mm}$ printing conditions for the PLA-Graphene.

Table 3 shows the optimum 3D printing parameters for the lowest dimensional errors for each build orientation and measurement axis. The optimum values of dimensional deviations on all axis (X, Y, Z) for the three build orientations were found at the interval [-54, 41.3] μm . Except for the X-axis in the flat orientation, where minimum dimensional errors increased significantly, values of 163.3 μm and 301.3 μm were obtained for PLA-3D and PLA-Graphene, respectively. This demonstrated that low value deviations could be achieved in all build orientations and on all axes with no significant differences between filament materials, except for the X-axis in the flat orientation, where higher dimensional deviation was observed in both filament materials. As shown in Table 3, a clear pattern in the selection of the optimum layer thickness was not found. Medium and high feed rates were found to be optimal in most cases, which would translate to increased productivity in manufacturing parts. As for layer thickness, low values of this parameter achieved the lowest dimensional deviations. However, a clear pattern could not be extracted for the on-edge and upright orientations.

3.2. Flatness error

For the evaluation of the flatness error, experimental data were characterized by multiple regression. Table 4 shows the adjusted coefficient of determination (R^2_{adj}), and Pearson's correlation coefficient (PCC) for the best multiple regression model obtained. The independent variables were the 3D printing parameters (Fr and Lt), and the dependent variable was the root mean square flatness deviation ($Fltq$). Regression models were obtained for both the PLA-3D and PLA-Graphene filaments, three measurement axes (X, Y, Z), and three build orientations (F, O, U). As shown in Table 4, three models obtained high R^2_{adj} values, above 80%, one model had a moderate R^2_{adj} of ~69%, and two models achieved R^2_{adj} values below 22%. In the latter two cases, the flatness error could not be characterized by regression models due to the low linearity (PCC) of 3D printing parameters versus the flatness error (see Table 4). As with the dimensional error analysis (Table 2), the lack of uniformity in the results obtained by multiple regression models indicated this technique was clearly not suitable for characterizing the flatness error. Therefore, ANNs were applied to obtain response surfaces.

The behaviour of the flatness error according to the 3D printing parameters for the three build orientations of both PLA-3D and PLA-Graphene filaments are shown in Fig. 5. Build orientation was

Table 3
Optimum dimensional deviations for both the PLA-3D and PLA-Graphene filaments.

Material	Axis	Build orientation									
			Flat			On-Edge			Upright		
			Fr (mm/s)	Lt (mm)	ΔD (μm)	Fr (mm/s)	Lt (mm)	ΔD (μm)	Fr (mm/s)	Lt (mm)	ΔD (μm)
PLA-3D	X	80	0.06	163.3	80	0.06	20.0	50	0.12	-7.0	
	Y	50	0.06	25.0	50	0.24	41.3	20	0.24	-7.6	
	Z	50	0.18	2.0	50	0.18	-1.6	50	0.18	0.0	
PLA-Graphene	X	80	0.06	301.3	50	0.06	5.5	50	0.06	-20.0	
	Y	50	0.06	-31.3	50	0.18	-54.0	80	0.12	2.6	
	Z	20	0.12	-52.0	80	0.06	-8.6	50	0.24	-11.0	

Table 4

Adjusted coefficient of determination (R^2_{adj}) and Pearson's correlation coefficient (PCC) for the flatness error ($Fltq$).

Material	Parameter	Flat		On-edge		Upright	
		R^2_{adj} (%)	PCC	R^2_{adj} (%)	PCC	R^2_{adj} (%)	PCC
PLA-3D	Fr	88.40	0.431	21.51	-0.596	84.12	0.149
	Lt		0.844		0.188		0.899
PLA-Graphene	Fr	81.19	0.043	69.16	0.044	12.31	-0.013
	Lt		0.765		-0.262		0.185

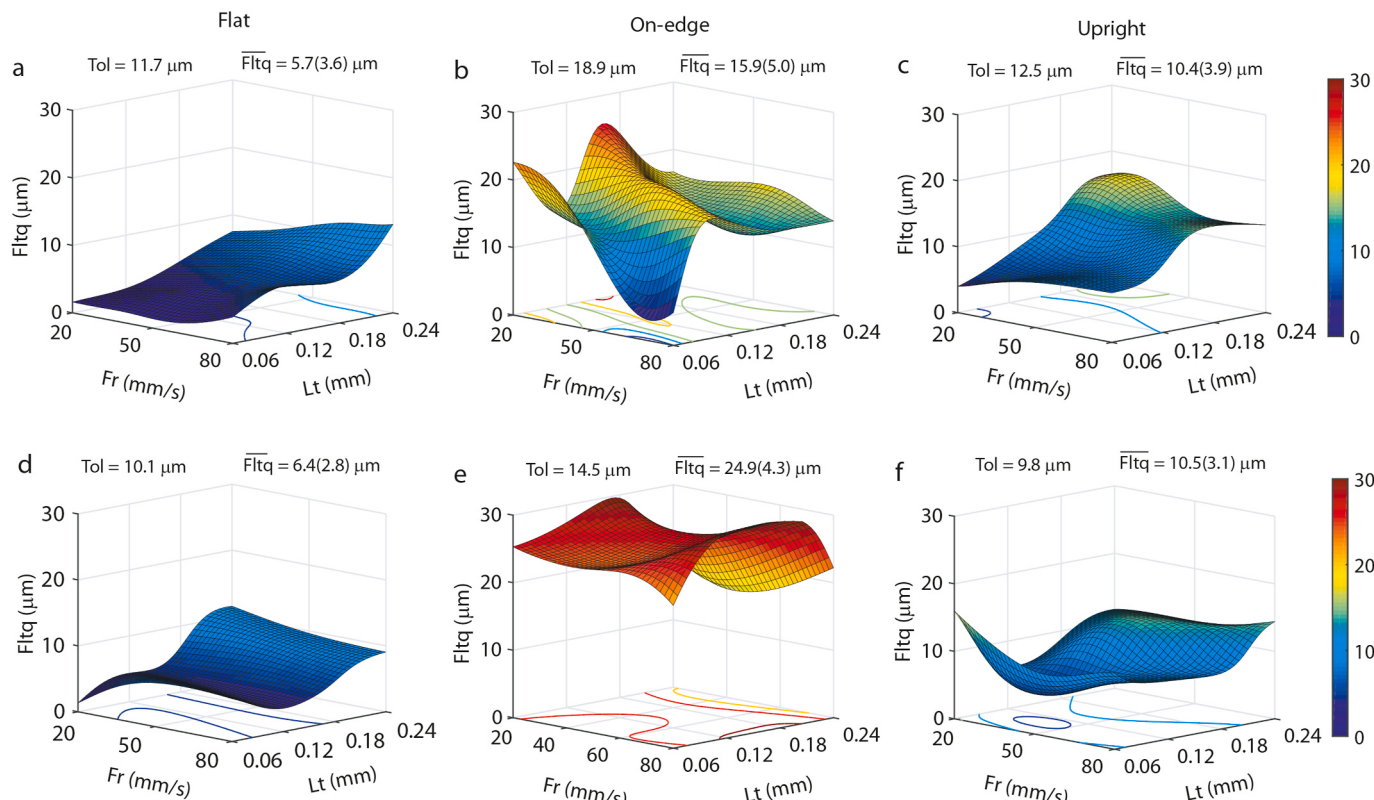


Fig. 5. Response surface obtained by ANN for flatness error ($Fltq$): PLA-3D (a, b, c), and PLA-Graphene (d, e, f) filaments.

observed to significantly influence the flatness error. In general, both materials obtained the best behaviour for the flat orientation (Fig. 5a and d), with $Fltq$ values lower than 13 μm for all of the tested conditions. In the flat orientation, the materials exhibited differences in behaviours in $Fltq$ according to the printing parameters. The PLA-3D material (Fig. 5a) showed the best results for the smallest layer thicknesses and the slowest feed rate, obtaining a minimum $Fltq$ of 1.6 μm with $Fr = 20$ mm/s and $Lt = 0.06$ mm. A quasi-linear growth in flatness was observed by increasing the Fr and Lt , in particular for the fastest feed rate of 80 mm/s, obtaining a maximum of 13.1 μm with the largest layer thickness ($Lt = 0.24$ mm). For the PLA-Graphene (Fig. 5d) the feed rate had no significant influence on the flatness error in 0.12, 0.16, and 0.24 mm layer thicknesses, but at the slowest feed rate of 20 m/s a significant decrease in $Fltq$ was observed with the lowest thickness ($Lt = 0.06$ mm), obtaining a minimum flatness error value of 1.3 μm . Regardless of the differences, both the PLA-3D and the PLA-Graphene filaments obtained similar mean $Fltq$ values of 5.7 ± 3.6 μm and 6.4 ± 2.8 μm , respectively.

The largest flatness error was obtained for the on-edge orientation (Fig. 5b and e) in both filament materials, particularly for the PLA-Graphene, with $Fltq$ values above 25 μm for most of the 3D printing conditions under analysis. The PLA-3D (Fig. 5b) showed a non-linear behaviour without any pattern trend in relation to 3D printing parameters, with $Fltq$ values ranging from 4.8 μm to 23.8 μm , and a mean value

of 15.9(5.0) μm . As shown in Fig. 5b high flatness error values of ~ 23 μm were reached at the slowest feed rate of 20 mm/s for 0.06 mm and 0.18 mm layer thicknesses. A feed rate of 80 mm/s produced a sharp decline in the flatness error in the smallest layer thickness, with a minimum absolute $Fltq$ of 4.8 μm . The PLA-Graphene (Fig. 5e) obtained a more uniform distribution except for high layer thickness, where a significant decrease in $Fltq$ was observed. For this material, flatness error values ranged from 16.4 μm to 30.9 μm , with a mean value of 24.9(4.3) μm .

The upright orientation (Fig. 5c and f) showed a non-linear behaviour, with a good flatness error (3.9 μm and 6.1 μm), and higher values (16.5 μm and 15.9 μm) of $Fltq$ according to the 3D printing conditions in both PLA-based materials. For the upright orientation, both PLA-3D and PLA-Graphene materials depicted completely different behaviours according to the printing parameters, nevertheless, both achieved similar mean flatness errors with values of 10.4(43.9) μm and 10.5(3.1) μm , respectively. For PLA-3D (Fig. 5c), the best results were obtained for the smallest layer thickness of 0.06 mm, with flatness errors ranging from 3.9 μm for $Fr = 20$ mm/s to 7.4 μm for $Fr = 80$ mm/s. Furthermore, a moderate interaction between the Fr and Lt printing parameters was found, with $Fltq$ increasing as layer thickness increased, particularly for the slowest feed rate of 20 mm/s, reaching a maximum absolute flatness error value of 16.5 μm . The PLA-Graphene (Fig. 5f) showed the

minimum flatness error for a layer thickness of 0.12 mm, with the flatness error increasing in the other ranges of layer thickness, and a minimum absolute value of 6.1 μm for $Fr = 50 \text{ mm/s}$, and a maximum absolute value of 15.9 μm for $Fr = 50 \text{ mm/s}$ and $Lt = 0.06 \text{ mm}$.

Table 5 summarizes the optimum 3D printing parameters for the lowest flatness errors for each build orientation. As shown, the PLA-3D obtained the best $Fltq$ values at a low layer thickness, whilst the feed rate exhibited no clear pattern. As for the PLA-Graphene, a clear pattern could not be extracted for the 3D printing parameters. Both materials obtained similar results in the flat position, but in the on edge and upright orientation, PLA-3D showed better results, particularly in the on edge orientation.

In order to analyse the flatness error behaviour, the surface 3D microgeometry (unfiltered surface texture components) of samples with the minimum and maximum flatness error in each build orientation for both PLA-3D and PLA-Graphene materials was studied. **Fig. 6** shows the 3D surface topography the minimum and maximum flatness error samples for each build orientation of both PLA-3D and PLA-Graphene filaments. The surface topography with the best flatness behaviour was obtained in the flat build orientation with the smallest layer thickness, with no significant differences between PLA-3D (**Fig. 6a**) and PLA-Graphene (**Fig. 6g**), with maximum peaks of $\sim 20 \mu\text{m}$ in both cases. In this build orientation, the samples with the maximum $Fltq$ values were obtained for the largest layer thickness ($Lt = 0.24 \text{ mm}$) PLA-3D (**Fig. 6d**) and PLA-Graphene (**Fig. 6j**), and both showed a deep valley in the central area with the maximum heights at the corners. This phenomenon was mainly caused by the cooling procedure, strongly influenced by the layer fill pattern and layer thickness. In the flat orientation, all layers were printed on the X-Y plane from the centre to the edge, producing residual stresses that severely affected flatness, particularly in the largest layer thickness.

For the on-edge and upright orientations, transversal waviness in a direction orthogonal to filament extrusion was observed; this transversal waviness negatively affected the flatness error. This phenomenon was due to the cylindricity defect of the threaded spindle for the vertical movement of the build plate [4]. In the on-edge orientation, the surface topography of the minimum flatness samples (**Fig. 6b** and **h**) showed both surfaces exhibited transversal waviness, but PLA-3D (**Fig. 6b**) obtained a smoother surface with maximum waviness peaks of $\sim 40 \mu\text{m}$, whereas the PLA-Graphene (**Fig. 6h**) reached peaks over $\sim 100 \mu\text{m}$. This indicated that transversal waviness affected the PLA-Graphene more than the PLA-3D. In this orientation, the surface topography for the maximum flatness samples (**Fig. 6e** and **k**) exhibited a similar behaviour, with maximum peaks of $140 \mu\text{m}$ (**Fig. 6e**) and $160 \mu\text{m}$ (**Fig. 6k**) for both the PLA-3D and PLA-Graphene filaments, respectively.

In the upright orientation, all surface topographies exhibited transversal waviness, which was more pronounced in PLA-3D (**Fig. 6f**). Similar to the on-edge orientation, in the minimum flatness samples (**Fig. 6c** and **i**) the PLA-3D showed a smoother surface topography with peaks of $\sim 30 \mu\text{m}$ (**Fig. 6c**), whereas the PLA-Graphene depicted peaks of $\sim 80 \mu\text{m}$ (**Fig. 6f**). As for the surfaces of the maximum flatness samples (**Fig. 6f** and **l**), both filament materials reached similar maximum peaks of $\sim 120 \mu\text{m}$, but these were obtained through different phenomena. For the PLA-3D (**Fig. 6f**) this maximum peak was reached mainly due to transversal waviness, nevertheless, the PLA-Graphene (**Fig. 6l**) obtained a surface bending similar to the one in the flat orientation.

Table 5
Optimum flatness error for both the PLA-3D and PLA-Graphene filaments.

Material	Build orientation						Fr (mm/s)	Lt (mm)	$Fltq$ (μm)			
	Flat			On-Edge								
	Fr (mm/s)	Lt (mm)	$Fltq$ (μm)	Fr (mm/s)	Lt (mm)	$Fltq$ (μm)						
PLA-3D	50	0.06	1.3	80	0.06	4.8	20	0.06	3.9			
PLA-Graphene	20	0.06	1.3	50	0.24	16.4	50	0.12	6.1			

3.3. Surface roughness

Surface roughness was evaluated by the arithmetic mean height (S_a), and the maximum heights of peaks and valleys (S_z) parameters. The statistical analysis of S_a for both the PLA-3D and PLA-Graphene filaments showed higher PCC for layer thickness, and higher values of R_{adj}^2 in the on-edge and upright orientations (**Table 6**). However, in the flat orientation, the PLA-Graphene regression models showed a low R_{adj}^2 and low linearity of the 3D printing parameters, specially feed rate. Thus, the lack of uniformity in the results presented in **Table 6** indicated that the regression technique is not appropriate to characterize the S_a parameter, and the use of the ANN method was warranted for developing response surfaces.

In order to assess the effect of the 3D printing parameters on surface finish, the behaviour of surface roughness (S_a) in the three building orientations for both PLA-3D and PLA-Graphene filaments was studied (**Fig. 7**). The best surface finish was obtained in the flat orientation (**Fig. 7a** and **d**), where roughness depended on the deposition and cooling of the melted filament, with lower values of S_a ranging from $1.1 \mu\text{m}$ – $4.3 \mu\text{m}$ for PLA-3D, and from $1.2 \mu\text{m}$ to $3.4 \mu\text{m}$ for the PLA-Graphene. In this orientation, the PLA-Graphene (**Fig. 7d**) showed a more uniform distribution than PLA-3D, with a S_a mean value of $1.8 (0.8) \mu\text{m}$ and $2.2(0.9) \mu\text{m}$, respectively, with most of the printing conditions reaching S_a values from $1.2 \mu\text{m}$ to $1.3 \mu\text{m}$. The PLA-3D (**Fig. 7a**) showed greater variability with increased layer thickness at lower feed rates adversely affecting surface roughness. For this material, the best behaviour was found at the smallest layer thickness (0.06 mm) with no significant influence of feed rate, and a minimum S_a value of $1.1 \mu\text{m}$ at the lowest feed rate (20 mm/s).

In the on-edge (**Fig. 7b** and **e**) and upright (**Fig. 7c** and **f**) orientations, where the texture generated depended on layer accumulation, the layer thickness severely affected surface roughness as depicted by the sharp increase in S_a according to this parameter, but with a smaller influence of feed rate. In the on-edge orientation, feed rate positively affected the S_a , with the best results at faster feed rates. In this orientation, the PLA-3D obtained better results than the PLA-Graphene, with optimum S_a values of $1.7 \mu\text{m}$ and $3.3 \mu\text{m}$, respectively. In the upright orientation, feed rate had no effect on surface roughness, and significant differences between materials were not found. The PLA-3D obtained the minimum S_a value of $1.5 \mu\text{m}$ at $Fr = 80 \text{ mm/s}$, whilst for the PLA-Graphene the best result was at $Fr = 20 \text{ mm/s}$ with a S_a value of $2.1 \mu\text{m}$. In short, both materials showed similar results in surface finish.

The effect of build orientation on roughness (S_a) was mainly caused by the deposition and cooling of the melted filament. In order to verify this aspect, **Fig. 8** and **Fig. 9** show PLA-3D extracted profiles of a perpendicular section of the filament in both the flat and upright orientations, respectively, using a constant feed rate of 20 mm/s . The differences between the minimum (0.06 mm) and maximum (0.24 mm) layer thicknesses observed were much higher for the upright than for the flat build orientation. In the flat orientation, the maximum amplitudes were $\pm 2.5 \mu\text{m}$ and $\pm 10 \mu\text{m}$ for $Lt = 0.06 \text{ mm}$ and $Lt = 0.24 \text{ mm}$, respectively; whilst in the upright orientation the variation was from $\pm 5 \mu\text{m}$ to $\pm 25 \mu\text{m}$. When texture was evaluated in the flat orientation, roughness depended on the nozzle diameter and the layer thickness. As shown in **Fig. 8**, with the nozzle diameter fixed at 0.4 mm , most of the crushing of the molten filament occurred at the lowest layer thickness,

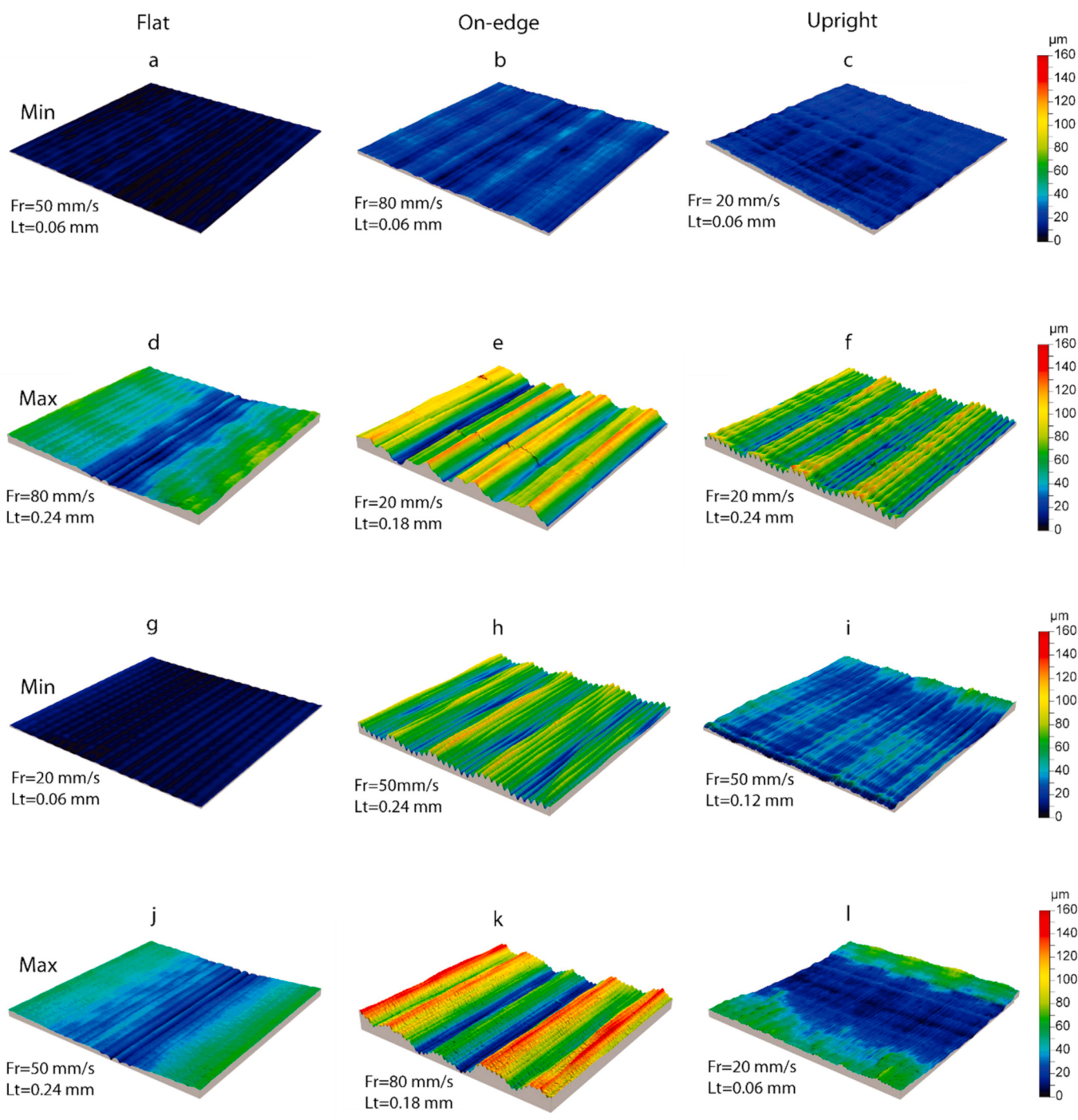


Fig. 6. 3D surface topography of the minimum and maximum flatness error samples for each build orientation: PLA-3D (from a to f), and PLA-Graphene (from g to l) filaments.

Table 6

Adjusted coefficient of determination (R^2_{adj}) and Pearson's correlation coefficient (PCC) for S_a parameter.

Material	Parameter	Flat		On-edge		Upright	
		R^2_{adj} (%)	PCC	R^2_{adj} (%)	PCC	R^2_{adj} (%)	PCC
PLA-3D	Fr	67.5	-0.370	86.2	-0.153	94.7	-0.084
	Lt		0.618		0.879		0.925
PLA-Graphene	S	24.4	-0.215	94.6	-0.158	98.4	-0.036
	Fr		0.564		0.854		0.937

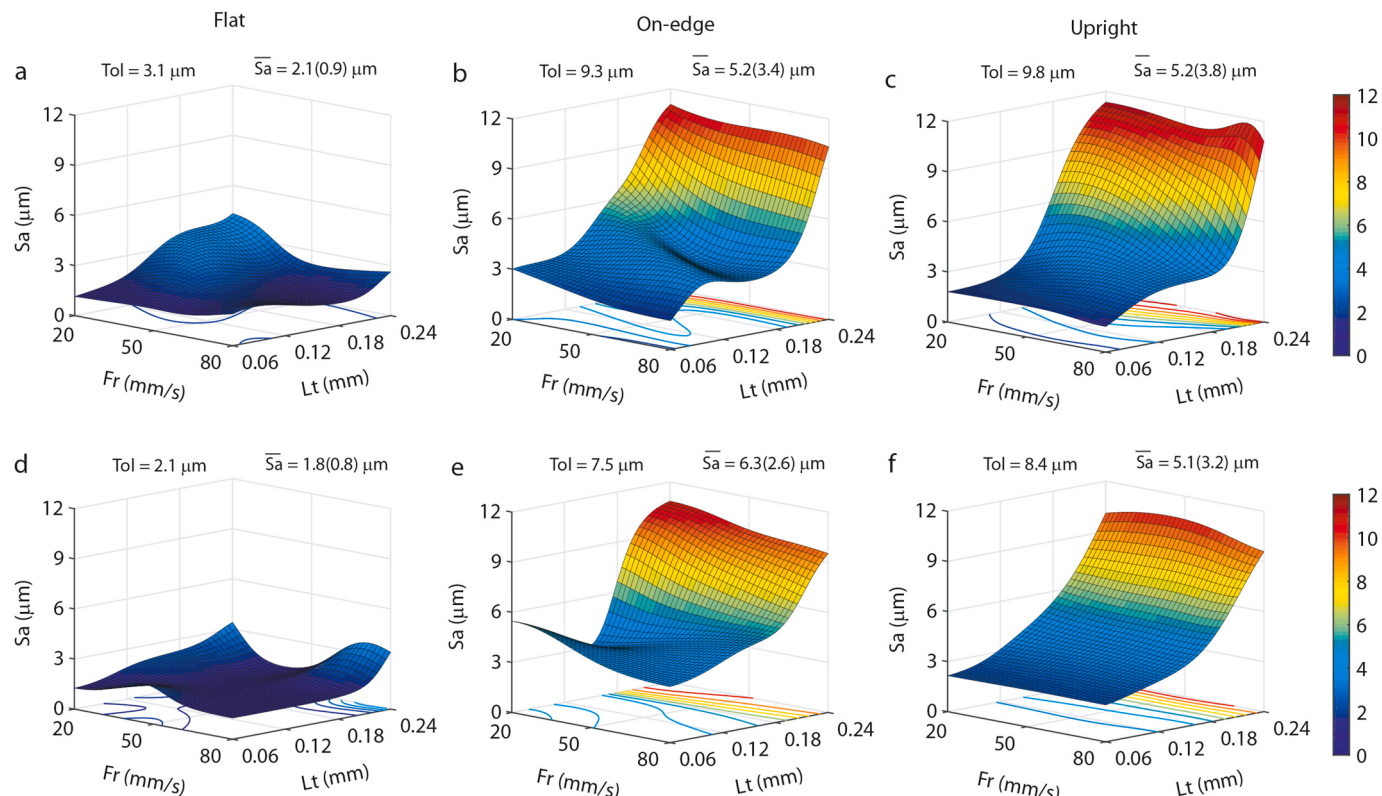


Fig. 7. Response surfaces obtained by ANN for roughness (S_a): PLA-3D (a, b, c), and PLA-Graphene (d, e, f) filaments.

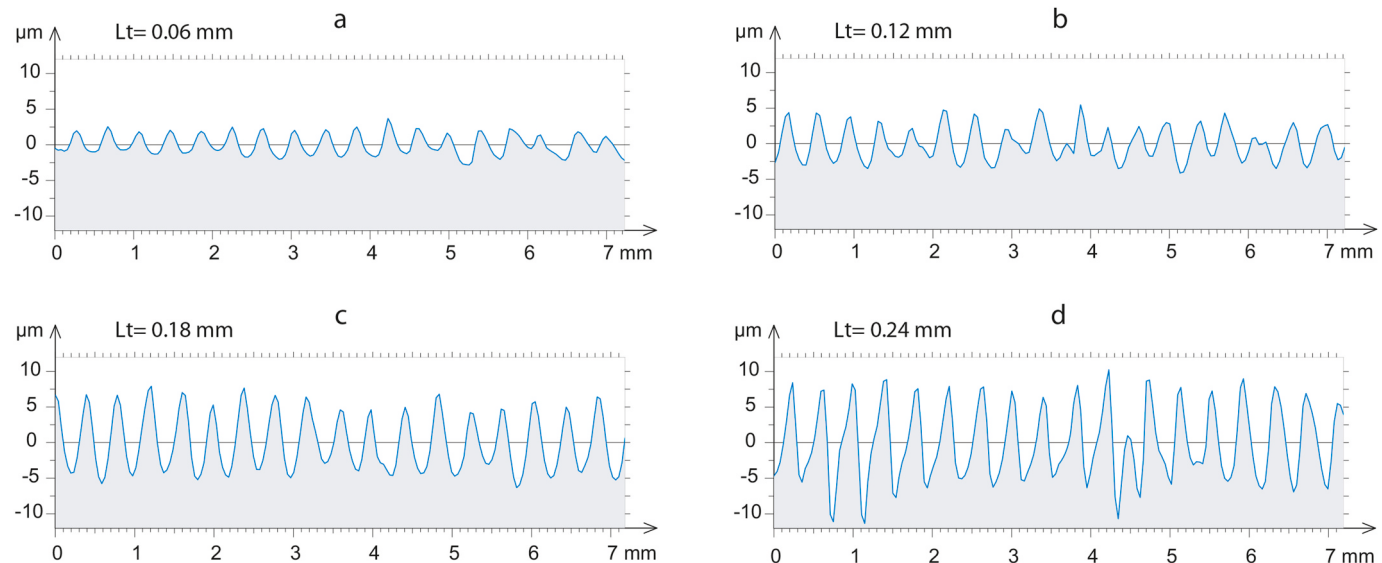


Fig. 8. Profile extractions in the flat orientation for PLA-3D filament with $Fr = 20 \text{ mm/s}$: a) $Lt = 0.06 \text{ mm}$, b) $Lt = 0.12 \text{ mm}$, c) $Lt = 0.18 \text{ mm}$, and d) $Lt = 0.24 \text{ mm}$.

with more filling of the gaps between contiguous filaments. For the upright and on-edge orientation (Fig. 9), only layer thickness affected surface roughness with significant differences in this parameter.

For the maximum heights of peaks and valleys the Sz parameter, the low adjustments of some regression models and the low linearity (Table 7) warranted the need for assessing the response surfaces using the ANN method, as in the previous cases.

Fig. 10 shows the evolution of the Sz parameter according to 3D printing parameters in each build orientation for both PLA-3D and PLA-Graphene materials. In general terms, the behaviour of the Sz parameter

was correlated to the Sa parameter, showing a similar trend in all response surfaces. For both materials, once again the best results were achieved for the flat orientation (Fig. 10a and d), with Sz minimum values of $8 \mu\text{m}$ and $10.3 \mu\text{m}$ for PLA-3D and PLA-Graphene, respectively, obtained at the lowest feed rate (20 m/s) and smallest layer thickness (0.06 mm). In this orientation, as opposed to the Sa parameter, the PLA-Graphene showed greater variations of Sz compared to PLA-3D, reaching a Sz maximum of $33.6 \mu\text{m}$ at $Fr = 50 \text{ m/s}$ and $Lt = 0.06 \text{ mm}$. In the on-edge orientation, PLA-3D (Fig. 10b) obtained the best results at $50 \leq Fr \leq 80 \text{ mm/s}$ and $0.06 \leq Lt \leq 0.12 \text{ mm}$, reaching a Sz minimum value

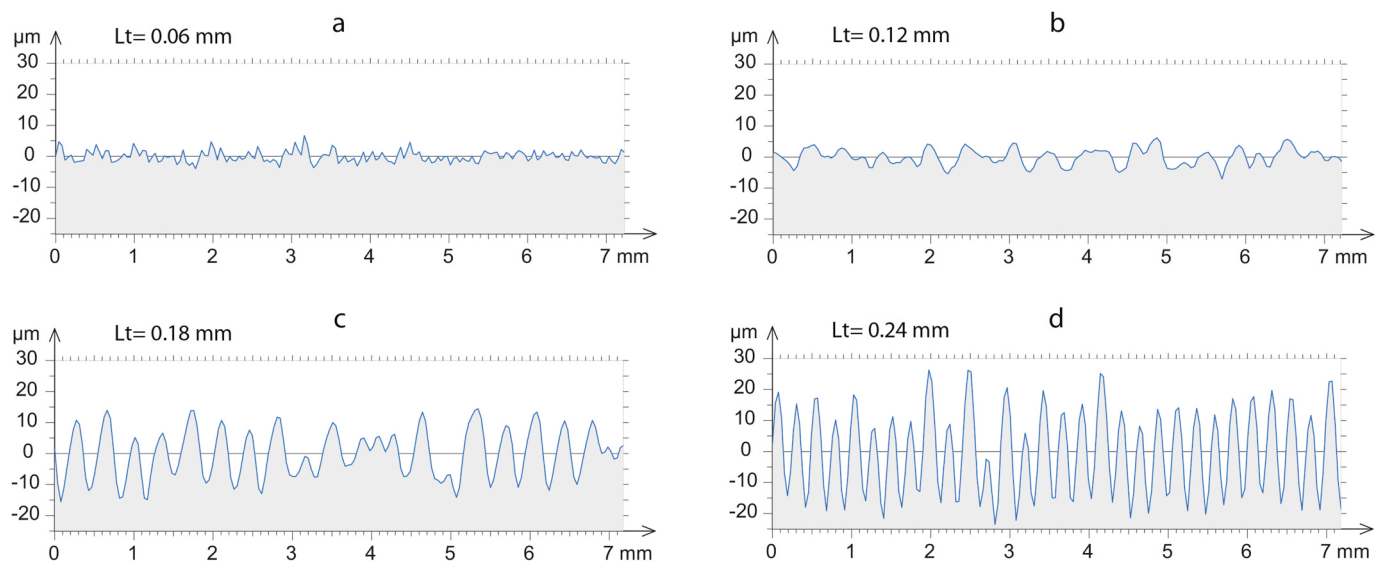


Fig. 9. Profile extractions in the upright orientation for PLA-3D filament with $Fr = 20 \text{ mm/s}$: a) $Lt = 0.06 \text{ mm}$, b) $Lt = 0.12 \text{ mm}$, c) $Lt = 0.18 \text{ mm}$, and d) $Lt = 0.24 \text{ mm}$.

Table 7

Adjusted coefficient of determination (R^2_{adj}) and Pearson's correlation coefficient (PCC) for Sz parameter.

Material	Parameter	Flat		On-edge		Upright	
		R^2_{adj} (%)	PCC	R^2_{adj} (%)	PCC	R^2_{adj} (%)	PCC
PLA-3D	Fr	33.1	-0.035	73.4	-0.383	92.8	-0.112
	Lt		0.571		0.740		0.931
PLA-Graphene	Fr	23.2	0.093	49.2	-0.184	83.4	-0.196
	Lt		0.486		0.310		0.901

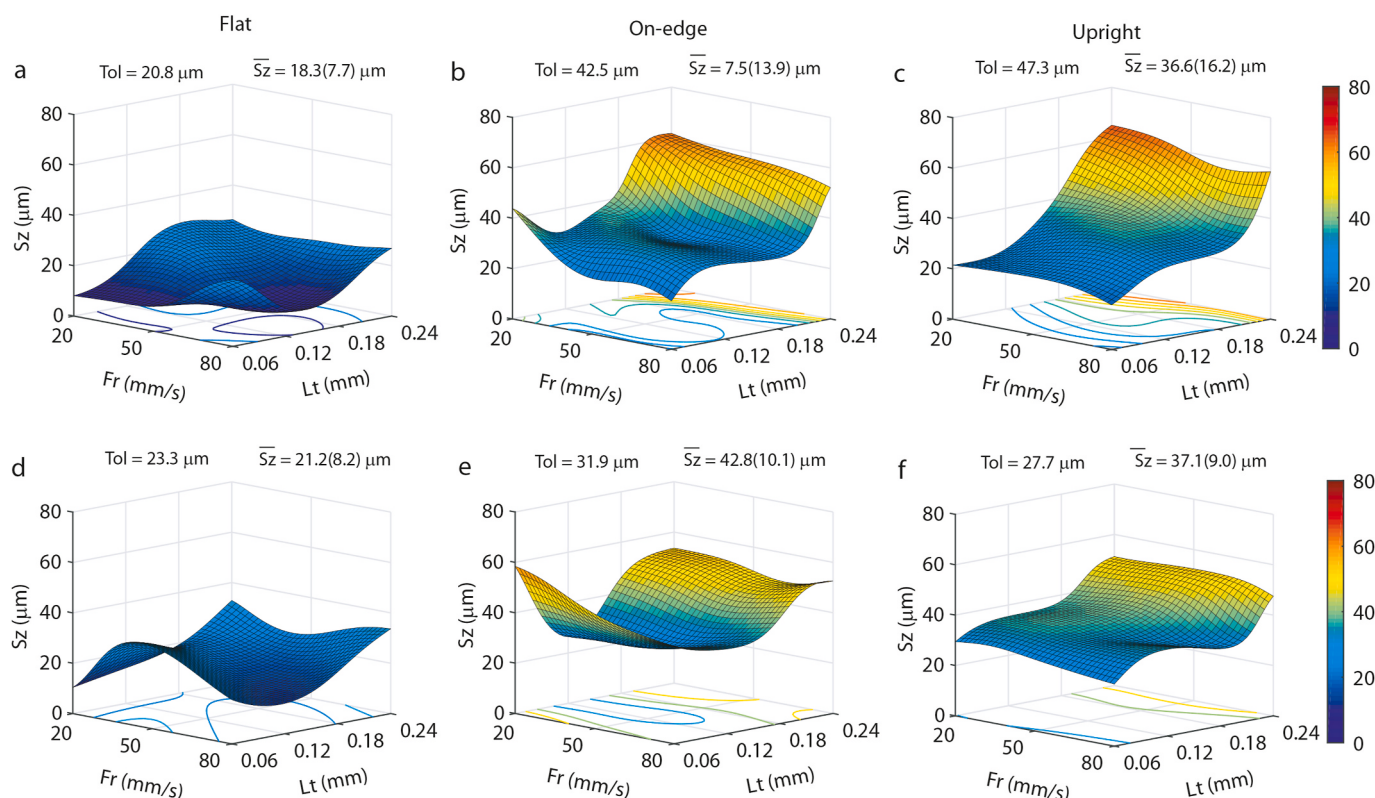


Fig. 10. Response surfaces obtained by ANN for roughness (Sz): PLA-3D (a, b, c), and PLA-Graphene (d, e, f) filaments.

of $19.1 \mu\text{m}$ at $Fr = 80 \text{ mm/s}$ and $Lt = 0.06 \text{ mm}$. A different trend was observed in the PLA-Graphene (Fig. 10e), the best results being obtained at $Fr = 20 \text{ mm/s}$ and $Lt = 0.12 \text{ mm}$ with a Sz value of $26.4 \mu\text{m}$. In the upright orientation, a high quasi-linear growth of Sz was observed with increased layer thickness, with no significant influence of feed rate for the PLA-3D material (Fig. 10c). Similarly, the Sz also increased in the PLA-Graphene with increased layer thickness but to a lesser extent (Fig. 10d). Both materials obtained the best results at the lowest layer thickness (0.06 mm) and fastest feed rate (80 mm/s), with minimum values of $17.7 \mu\text{m}$ and $24.6 \mu\text{m}$ for PLA-3D and PLA-Graphene, respectively.

Table 8 summarizes the optimum 3D printing parameters for the lowest surface roughness (Sa and Sz) for each build orientation. As shown, both materials obtained similar Sa and Sz values for each build orientation, but slightly better values for PLA-3D in the tree positions. The optimum Sa and Sz values were always obtained with the smallest layer thickness ($Lt = 0.06 \text{ mm}$), whilst the behaviour of the feed rate differed according to the build orientation. In general, the best results in the flat position were obtained at the slowest feed rate, whereas in the on edge and upright orientations the optimum results were reached at the fastest feed rate ($Fr = 80 \text{ mm/s}$).

Fig. 11 shows the 3D surface roughness topography (filtered using a Gaussian low-pass filter at 0.8 mm cut-off) of the minimum and maximum roughness samples for each build orientation of both PLA-3D and PLA-Graphene filaments. The surfaces with lowest peak heights were obtained in the flat orientation for both PLA-3D (Fig. 11a) and PLA-Graphene (Fig. 11g), indicating the surfaces perpendicular to the extruder were the best option for achieving low surface roughness. In this orientation, significant differences between materials were not found, and the minimum roughness samples showed maximum peak heights of $5 \mu\text{m}$ in both cases. However, for the maximum roughness samples, the PLA-3D (Fig. 11d) showed slightly better behaviour with maximum peak heights of $15 \mu\text{m}$ compared to the higher peaks of $25 \mu\text{m}$ in the PLA-Graphene (Fig. 11j), mainly due to deficient filament deposition in the central area. It should be noted that for the largest layer thickness, PLA-Graphene surfaces showed a granular aspect due to high concentrations of graphene particles in this layer thickness.

In the on-edge and upright build orientations, the minimum roughness samples showed the best results for the PLA-3D, with maximum peak heights of $15 \mu\text{m}$ for the on-edge (Fig. 11b), and $10 \mu\text{m}$ for the upright (Fig. 11c) orientations. For the PLA-Graphene, the maximum peak heights reached values of $30 \mu\text{m}$ for the on-edge (Fig. 11h) and $25 \mu\text{m}$ for upright orientations (Fig. 11i). As for the maximum roughness samples in the on-edge and upright orientations, all samples showed high peak heights. The PLA-3D showed the worst results, particularly in the upright orientation (Fig. 11f), where surface roughness exhibited an irregular behaviour with maximum peak heights of $65 \mu\text{m}$ in several cases. In the on-edge orientation, PLA-3D also showed maximum peak heights of $65 \mu\text{m}$ but to a lesser extent (Fig. 11e). The PLA-Graphene obtained more uniform surfaces with no significant differences between the on-edge (Fig. 11k) and upright (Fig. 11l) orientations, with lower peak heights reaching maximum peaks of $55 \mu\text{m}$ in only a few filaments.

4. Conclusions

In this study, the geometric properties of two PLA-based filaments in functional products printed by 3D FFF were compared. By varying three printing parameters – layer thickness, feed rate, and build orientation – their effect on the dimensional accuracy, flatness error, surface texture, and surface roughness were analysed. Two different commercial PLA-based filaments were tested: an unreinforced PLA polymer specially designed for 3D printers (PLA-3D), and a graphene nanoplatelet reinforced PLA composite (PLA-Graphene). All specimens were manufactured with a BQ Witbox 3D printer, using a full factorial experimental design with 3 factors at 3 and 4 levels. The analysis methodology included analysis of variance, artificial neural networks, and response surfaces.

The results showed that on the X-Y plane, dimensional accuracy was mainly affected by build orientation as this geometrical property was directly related to the length of the movement of the extruder. An increase in the layer area on the X-Y plane increased dimensional deviation owing to the longer displacements of the extruder accumulating positioning errors. However, on the Z-axis the accumulation of layers did not significantly affect the dimensional accuracy in each tested build orientation.

The upright orientation was not significantly influenced by any of the printing parameters analysed. In the flat orientation, the PLA-Graphene was affected by layer thickness, with an increase in this parameter negatively affecting dimensional accuracy. However, for PLA-3D, both feed rate and layer thickness showed dimensional deviations, but with no clear pattern of behaviour. For the on-edge orientation, only the Y-axis was affected by the printing parameters, with an increase in both layer thickness and feed rate improving dimensional accuracy. The Z-axis was not affected by the printing parameters, providing the best tolerances in most cases.

The minimum flatness error was obtained in the flat orientation, which mainly depended on the solidification conditions of the filaments. In contrast, the flatness errors on surfaces formed by accumulated layers (in on-edge and upright orientations) increased under most of the printing conditions tested. This behaviour was mainly attributed to the transversal waviness detected in the direction perpendicular to the extrusion trajectory, generated by cylindricity defects in the threaded spindle that vertically moved the build plate.

Surface roughness exhibited two different behaviours according to build orientation. In the on-edge and upright orientations, roughness (Sa and Sz parameters) showed a quasi-linear growth with increasing layer thickness, but with no significant effect of feed rate. In the flat orientation, filament crushing by the extruder in each layer produced lower values of surface roughness in all printing conditions tested.

Finally, the two analysed PLA-based filaments showed no significant variations in geometric properties during processing by FFF additive manufacturing. However, PLA-Graphene filaments improved mechanical, electrical, and thermal properties [17–19], without the loss of geometric quality, making it an ideal material for processing by FFF additive manufacturing.

Table 8

Optimum surface roughness (Sa and Sz) for both the PLA-3D and PLA-Graphene filaments.

Material	Parameter	Build orientation								
		Flat			On-Edge			Upright		
		$Fr (\text{mm/s})$	$Lt (\text{mm})$	$Fltq (\mu\text{m})$	$Fr (\text{mm/s})$	$Lt (\text{mm})$	$Fltq (\mu\text{m})$	$Fr (\text{mm/s})$	$Lt (\text{mm})$	$Fltq (\mu\text{m})$
PLA-3D	Sa	20	0.06	1.1	80	0.06	1.7	80	0.06	1.5
	Sz	20	0.06	8.1	80	0.06	19.1	80	0.06	17.7
PLA-Graphene	Sa	20	0.06	1.2	80	0.06	3.3	20	0.06	2.1
	Sz	20	0.06	10.3	20	0.12	26.4	80	0.06	24.6

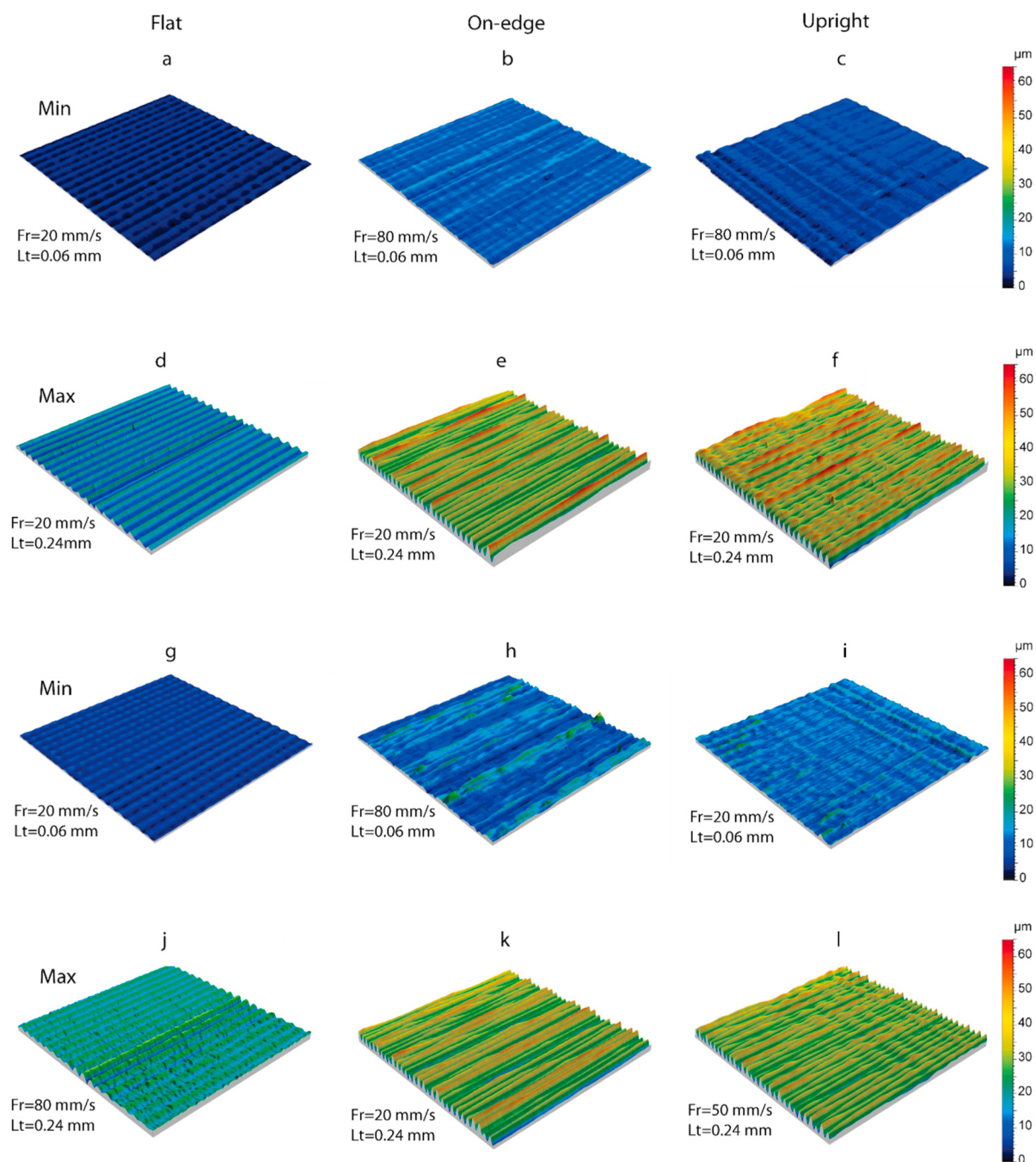


Fig. 11. 3D surface roughness topography: PLA-3D (from a to f), and PLA-Graphene (from g to l) filaments.

Author statement

E. García, P.J. Núñez, J.M. Chacón, M.A. Caminero and S. Kamarthi: Conceptualization; E. García, P.J. Núñez, J.M. Chacón and M.A. Caminero: Data curation; E. García and P.J. Núñez: Formal analysis; P.J. Núñez, J.M. Chacón and M.A. Caminero: Funding acquisition; E. García, P.J. Núñez, J.M. Chacón, M.A. Caminero and S. Kamarthi: Investigation; E. García and P.J. Núñez: Methodology; P.J. Núñez: Project administration; P.J. Núñez, J.M. Chacón and M.A. Caminero: Resources; E. García: Software; S. Kamarthi: Supervision; E. García, P.J. Núñez, J.M. Chacón and M.A. Caminero: Validation; E. García, P.J. Núñez: Visualization; E. García and P.J. Núñez: Writing - original draft; E. García, P.J. Núñez, J.M. Chacón, M.A. Caminero and S. Kamarthi: Writing - review & editing.

Declaration of competing interest

The authors declare that they have no known competing financial interests or personal relationships that could have appeared to influence the work reported in this paper.

Acknowledgments

The research was supported by the Spanish Ministry of Science and Innovation (research grant PID2019-104586RB-I00), and Castilla-La Mancha Community Council (research grants SBPLY/19/180501/000247 and SBPLY/19/180501/000170), University of Castilla-La Mancha (research grant 2020-GRIN-28758), and co-financed by the ERDF (European Regional Development Fund). Finally, we thank the

referees for their valuable suggestions, which improved this article.

Appendix A. Supplementary data

Supplementary data to this article can be found online at <https://doi.org/10.1016/j.polymertesting.2020.106860>.

References

- [1] F. Alam, K.M. Varadarajan, S. Kumar, 3D printed polylactic acid nanocomposite scaffolds for tissue engineering applications, *Polym. Test.* 81 (2020) 106203, <https://doi.org/10.1016/j.polymertesting.2019.106203>.
- [2] F. Arbeiter, M. Spoerl, J. Wiener, A. Gosch, G. Pinter, Fracture mechanical characterization and lifetime estimation of near-homogeneous components produced by fused filament fabrication, *Polym. Test.* 66 (2018) 105–113, <https://doi.org/10.1016/j.polymertesting.2018.01.002>.
- [3] O. Ahmed, S. Hasan, J. Lal, Optimization of fused deposition modeling process parameters for dimensional accuracy using I-optimality criterion, *Measurement* 81 (2016) 174–196, <https://doi.org/10.1016/j.measurement.2015.12.011>.
- [4] E. García Plaza, P.J.N. López, M.A.C. Torija, J.M.C. Muñoz, Analysis of PLA geometric properties processed by FFF additive manufacturing: effects of process parameters and plate-extruder precision motion, *Polymers* 11 (2019) 1581, <https://doi.org/10.3390/polym11101581>.
- [5] T. Sonsalla, A.L. Moore, A.D. Radadia, L. Weiss, Printer orientation effects and performance of novel 3-D printable acrylonitrile butadiene styrene (ABS) composite filaments for thermal enhancement, *Polym. Test.* (2019), <https://doi.org/10.1016/j.polymertesting.2019.106125>.
- [6] C.R. Hatz, B. Msalleem, S. Aghilmardi, P. Brantner, F.M. Thieringer, Can an entry-level 3D printer create high-quality anatomical models? Accuracy assessment of mandibular models printed by a desktop 3D printer and a professional device, *Int. J. Oral Maxillofac. Surg.* (2019), <https://doi.org/10.1016/j.ijom.2019.03.962>.
- [7] D. Singh, R. Singh, K.S. Bopari, Development and surface improvement of FDM pattern based investment casting of biomedical implants: a state of art review, *J. Manuf. Process.* 31 (2018) 80–95, <https://doi.org/10.1016/j.jmapro.2017.10.026>.
- [8] S.H. Masood, Advances in fused deposition modeling, *Compr. Mater. Process.* (2014) 69–91, <https://doi.org/10.1016/B978-0-08-096352-1.01002-5>.
- [9] M.A. Caminero, J.M. Chacón, I. García-Moreno, J.M. Reverte, Interlaminar bonding performance of 3D printed continuous fibre reinforced thermoplastic composites using fused deposition modelling, *Polym. Test.* (2018), <https://doi.org/10.1016/j.polymertesting.2018.04.038>.
- [10] S.K. Hedayati, A.H. Behravesh, S. Hasannia, A. Bagheri Saed, B. Akhouni, 3D printed PCL scaffold reinforced with continuous biodegradable fiber yarn: a study on mechanical and cell viability properties, *Polym. Test.* 83 (2020) 106347, <https://doi.org/10.1016/j.polymertesting.2020.106347>.
- [11] L.G. Blok, M.L. Longana, H. Yu, B.K.S. Woods, An investigation into 3D printing of fibre reinforced thermoplastic composites, *Addit. Manuf.* 22 (2018) 176–186, <https://doi.org/10.1016/j.addma.2018.04.039>.
- [12] N. Nawafleh, E. Celik, Additive manufacturing of short fiber reinforced thermoset composites with unprecedented mechanical performance, *Addit. Manuf.* 33 (2020) 101109, <https://doi.org/10.1016/j.addma.2020.101109>.
- [13] R.T.L. Ferreira, I.C. Amatte, T.A. Dutra, D. Bürger, Experimental characterization and micrography of 3D printed PLA and PLA reinforced with short carbon fibers, *Compos. B Eng.* 124 (2017) 88–100, <https://doi.org/10.1016/j.compscitech.2017.05.013>.
- [14] J.M. Chacón, M.A. Caminero, P.J. Núñez, E. García-Plaza, I. García-Moreno, J. M. Reverte, Additive manufacturing of continuous fibre reinforced thermoplastic composites using fused deposition modelling: effect of process parameters on mechanical properties, *Compos. Sci. Technol.* (2019), <https://doi.org/10.1016/j.compscitech.2019.107688>.
- [15] M.N. Jahangir, J. Cleeman, H.J. Hwang, R. Malhotra, Towards out-of-chamber damage-free fabrication of highly conductive nanoparticle-based circuits inside 3D printed thermally sensitive polymers, *Addit. Manuf.* 30 (2019), <https://doi.org/10.1016/j.addma.2019.100886>.
- [16] N.K. Roy, C.S. Foong, M.A. Cullinan, Effect of size, morphology, and synthesis method on the thermal and sintering properties of copper nanoparticles for use in microscale additive manufacturing processes, *Addit. Manuf.* 21 (2018) 17–29, <https://doi.org/10.1016/j.addma.2018.02.008>.
- [17] M.A. Caminero, J.M. Chacón, E. García-Plaza, P.J. Núñez, J.M. Reverte, J.P. Becar, Additive manufacturing of PLA-based composites using fused filament fabrication: effect of graphene nanoplatelet reinforcement on mechanical properties, dimensional accuracy and texture, *Polymers* 11 (2019) 799, <https://doi.org/10.3390/polym11050799>.
- [18] S. Singh, M. Singh, C. Prakash, M.K. Gupta, M. Mia, R. Singh, Optimization and reliability analysis to improve surface quality and mechanical characteristics of heat-treated fused filament fabricated parts, *Int. J. Adv. Manuf. Technol.* 102 (2019) 1521–1536, <https://doi.org/10.1007/s00170-018-03276-8>.
- [19] M.F. Arif, H. Alhashmi, K.M. Varadarajan, J.H. Koo, A.J. Hart, S. Kumar, Multifunctional performance of carbon nanotubes and graphene nanoplatelets reinforced PEEK composites enabled via FFF additive manufacturing, *Compos. B Eng.* (2019) 107625, <https://doi.org/10.1016/j.compositesb.2019.107625>.
- [20] M. Lay, N.L.N. Thajudin, Z.A.A. Hamid, A. Rusli, M.K. Abdullah, R.K. Shuib, Comparison of physical and mechanical properties of PLA, ABS and nylon 6 fabricated using fused deposition modeling and injection molding, *Compos. B Eng.* 176 (2019), <https://doi.org/10.1016/j.compositesb.2019.107341>.
- [21] V.T. Le, H. Paris, G. Mandil, Process planning for combined additive and subtractive manufacturing technologies in a remanufacturing context, *J. Manuf. Syst.* 44 (2017) 243–254, <https://doi.org/10.1016/j.jmssy.2017.06.003>.
- [22] M. Spoerl, C. Holzer, J. Gonzalez-Gutierrez, Material extrusion-based additive manufacturing of polypropylene: a review on how to improve dimensional inaccuracy and warpage, *J. Appl. Polym. Sci.* 137 (2020) 1–16, <https://doi.org/10.1002/app.48545>.
- [23] A. Kumar, R.K. Ohdar, S.S. Mahapatra, Improving dimensional accuracy of Fused Deposition Modelling processed part using grey Taguchi method, *Mater. Des.* 30 (2009) 4243–4252, <https://doi.org/10.1016/j.matdes.2009.04.030>.
- [24] R.K. Sahu, S.S. Mahapatra, A.K. Sood, A study on dimensional accuracy of fused deposition modeling (FDM) processed parts using fuzzy logic, *J. Manuf. Sci. Prod.* (2013), <https://doi.org/10.1515/jmsp-2013-0010>.
- [25] D.Y. Chang, B.H. Huang, Studies on profile error and extruding aperture for the RP parts using the fused deposition modeling process, *Int. J. Adv. Manuf. Technol.* 53 (2011) 1027–1037, <https://doi.org/10.1007/s00170-010-2882-1>.
- [26] A. Peng, X. Xiao, R. Yue, Process parameter optimization for fused deposition modeling using response surface methodology combined with fuzzy inference system, *Int. J. Adv. Manuf. Technol.* 73 (2014) 87–100, <https://doi.org/10.1007/s00170-014-5796-5>.
- [27] O. Ahmed, S. Hasan, J. Lal, Optimization of fused deposition modeling process parameters for dimensional accuracy using I-optimality criterion, *Measurement* 81 (2016) 174–196, <https://doi.org/10.1016/j.measurement.2015.12.011>.
- [28] M. Kaveh, M. Badrossamay, E. Porroozmehr, A. Hemasian Etefagh, Optimization of the printing parameters affecting dimensional accuracy and internal cavity for HIPS material used in fused deposition modeling processes, *J. Mater. Process. Technol.* 226 (2015) 280–286, <https://doi.org/10.1016/j.jmatprotec.2015.07.012>.
- [29] P. Geng, J. Zhao, W. Wu, W. Ye, Y. Wang, S. Wang, S. Zhang, Effects of extrusion speed and printing speed on the 3D printing stability of extruded PEEK filament, *J. Manuf. Process.* 37 (2019) 266–273, <https://doi.org/10.1016/j.jmapro.2018.11.023>.
- [30] A. Noriega, D. Blanco, B.J. Alvarez, A. Garcia, Dimensional accuracy improvement of FDM square cross-section parts using artificial neural networks and an optimization algorithm, *Int. J. Adv. Manuf. Technol.* 69 (2013) 2301–2313, <https://doi.org/10.1007/s00170-013-5196-2>.
- [31] C.-Y. Lee, C.-Y. Liu, The influence of forced-air cooling on a 3D printed PLA part manufactured by fused filament fabrication, *Addit. Manuf.* 25 (2019) 196–203, <https://doi.org/10.1016/j.addma.2018.11.012>.
- [32] L.M. Galantucci, I. Bodí, J. Kacani, F. Lavecchia, Analysis of dimensional performance for a 3D open-source printer based on fused deposition modeling technique, *Procedia CIRP* 28 (2015) 82–87, <https://doi.org/10.1016/j.procir.2015.04.014>.
- [33] M. Spoerl, C. Savandaiah, F. Arbeiter, G. Traxler, L. Cardon, C. Holzer, J. Sapkota, Anisotropic properties of oriented short carbon fibre filled polypropylene parts fabricated by extrusion-based additive manufacturing, *Composites Part A Appl. Sci. Manuf.* 113 (2018) 95–104, <https://doi.org/10.1016/j.compositesa.2018.06.018>.
- [34] M. Spoerl, F. Arbeiter, I. Raguz, G. Weingrill, T. Fischinger, G. Traxler, S. Schuschnigg, L. Cardon, C. Holzer, Polypropylene filled with glass spheres in extrusion-based additive manufacturing: effect of filler size and printing chamber temperature, *Macromol. Mater. Eng.* 303 (2018), <https://doi.org/10.1002/mame.201800179>.
- [35] L. Wang, W. Gramlich, D. Gardner, Y. Han, M. Tajvidi, Spray-dried cellulose nanofibril-reinforced polypropylene composites for extrusion-based additive manufacturing: nonisothermal crystallization kinetics and thermal expansion, *J. Compos. Sci.* 2 (2018) 7, <https://doi.org/10.3390/jcs2010007>.
- [36] A. Boschetto, L. Bottini, Design for manufacturing of surfaces to improve accuracy in Fused Deposition Modeling, *Robot. Comput. Integrated Manuf.* 37 (2016) 103–114, <https://doi.org/10.1016/j.rcim.2015.07.005>.
- [37] S. Mahmood, A.J. Qureshi, D. Talamona, Taguchi based process optimization for dimension and tolerance control for fused deposition modelling, *Addit. Manuf.* 21 (2018) 183–190, <https://doi.org/10.1016/j.addma.2018.03.009>.
- [38] A. Reyes-Rodríguez, R. Dorado-Vicente, R. Mayor-Vicario, Dimensional and form errors of PC parts printed via Fused Deposition Modelling, *Procedia Manuf.* 13 (2017) 880–887, <https://doi.org/10.1016/j.promfg.2017.09.149>.
- [39] P.J. Núñez, A. Rivas, E. García-Plaza, E. Beamu, A. Sanz-Lobera, Dimensional and surface texture characterization in fused deposition modelling (FDM) with ABS plus, *Procedia Eng.* 132 (2015) 856–863, <https://doi.org/10.1016/j.proeng.2015.12.570>.
- [40] N. Sajan, T.D. John, M. Sivadasan, N.K. Singh, An investigation on circularity error of components processed on Fused Deposition Modeling (FDM), *Mater. Today Proc.* 5 (2018) 1327–1334, <https://doi.org/10.1016/j.matpr.2017.11.218>.
- [41] D. Ahn, J.H. Kweon, S. Kwon, J. Song, S. Lee, Representation of surface roughness in fused deposition modeling, *J. Mater. Process. Technol.* 209 (2009) 5593–5600, <https://doi.org/10.1016/j.jmatprotec.2009.05.016>.
- [42] A. Boschetto, V. Giordano, F. Veniali, Modelling micro geometrical profiles in fused deposition process, *Int. J. Adv. Manuf. Technol.* 61 (2012) 945–956, <https://doi.org/10.1007/s00170-011-3744-1>.
- [43] A. Boschetto, V. Giordano, F. Veniali, Surface roughness prediction in fused deposition modelling by neural networks, *Int. J. Adv. Manuf. Technol.* 67 (2013) 2727–2742, <https://doi.org/10.1007/s00170-012-4687-x>.
- [44] A. Boschetto, V. Giordano, F. Veniali, 3D roughness profile model in fused deposition modelling, *Rapid Prototyp. J.* 19 (2013) 240–252, <https://doi.org/10.1108/13552541311323254>.

- [45] A. Boschetto, L. Bottini, F. Veniali, Integration of FDM surface quality modeling with process design, *Addit. Manuf.* 12 (2016) 334–344, <https://doi.org/10.1016/j.addma.2016.05.008>.
- [46] Y. Jin, H. Li, Y. He, J. Fu, Quantitative analysis of surface profile in fused deposition modeling, *Addit. Manuf.* 8 (2015) 142–148, <https://doi.org/10.1016/j.addma.2015.10.001>.
- [47] V. Reddy, O. Flys, A. Chaparala, C.E. Berrimi, V. Amogh, Study on surface texture of fused deposition modeling, *Procedia Manuf.* (2018) 16–18, <https://doi.org/10.1016/j.promfg.2018.06.108>, 00.
- [48] M. Mu, C.-Y. Ou, J. Wang, Y. Liu, Surface modification of prototypes in fused filament fabrication using chemical vapour smoothing, *Addit. Manuf.* (2019) 100972, <https://doi.org/10.1016/j.addma.2019.100972>.
- [49] ISO 12781-1, Geometrical Product Specifications (GPS) - Flatness - Part 1: Vocabulary and Parameters of Flatness, 2011.
- [50] ISO 25178-2, Geometrical Product Specifications (GPS) - Surface Texture: Areal - Part 2: Terms, Definitions and Surface Texture Parameters, 2012.